JGR Oceans

RESEARCH ARTICLE
10.1029/2020JC016901

Special Section:
Significant advances in ocean and climate sciences of the Pacific-Asian Marginal Seas

Nathalie F. Goodkin and Kristopher B. Karnauskas contributed equally.

Key Points:

- South China Sea (SCS) ocean transports are studied using a high-resolution regional ocean model and high-resolution global climate models
- The seasonally varying intermediate and deep layer water mass in the SCS originates in the central Pacific Ocean
- High-resolution global climate models predict pronounced changes in SCS transports in response to anthropogenic forcing

Supporting Information:

Supporting Information may be found in the online version of this article.

Correspondence to:

D. Samanta,
dhruba@ntu.edu.sg

Citation:

Samanta, D., Goodkin, N. F., & Karnauskas, K. B. (2021). Volume and heat transport in the South China Sea and maritime continent at present and the end of the 21st century. *Journal of Geophysical Research: Oceans*, *126*, e2020JC016901. https://doi.org/10.1029/2020JC016901

Received 16 OCT 2020
Accepted 17 AUG 2021

© 2021 The Authors.
This is an open access article under the terms of the Creative Commons Attribution-NonCommercial License, which permits use, distribution and reproduction in any medium, provided the original work is properly cited and is not used for commercial purposes.

Volume and Heat Transport in the South China Sea and Maritime Continent at Present and the End of the 21st Century

Dhrubajyoti Samanta[1,2], Nathalie F. Goodkin[1,2,3], and Kristopher B. Karnauskas[4,5]

[1]Asian School of the Environment, Nanyang Technological University, Singapore, Singapore, [2]Earth Observatory of Singapore, Nanyang Technological University, Singapore, Singapore, [3]Department of Earth and Planetary Sciences, American Museum of Natural History, New York, NY, USA, [4]Department of Atmospheric and Oceanic Sciences, University of Colorado Boulder, Boulder, CO, USA, [5]Cooperative Institute for Research in Environmental Sciences, University of Colorado Boulder, Boulder, CO, USA

Abstract Ocean transports through the Southeast Asian Seas connect the western tropical Pacific and Indian Oceans, thereby exerting an important role in regional and global climate. High-resolution regional ocean model simulations over the South China Sea (SCS) and maritime continent are used to study the mean and seasonally varying thermohaline structure and volume transport through the straits surrounding the SCS. Diversity in the vertical structure of these straits is not only indicative of the role of widely varying bathymetry but also strong seasonality associated with monsoonal currents. The presence of a Pacific water mass in intermediate and deep layers of the Luzon Strait points to a key pathway between the Pacific and Indian Oceans. Further, examining a suite of global, high-resolution model simulations reveals the projected changes in the regional upper ocean transports due to anthropogenic radiative forcing by the end of the 21st century. The global models predict an increase in heat and volume transport through the Luzon and Karimata Straits, and a decrease thereof through the Makassar and Lombok Straits by the end of the century. Overall, these changes impute additional net convergence of heat and volume in the SCS, a significant reduction of sea surface salinity and mixed layer depth, and an increase in the upper-ocean heat content of the region. As the SCS serves as a regional heat capacitor and is impacted by the global thermohaline circulation locally via Indonesian Throughflow, these predicted changes have the potential to impact climate over the Indo-Pacific region and globally.

Plain Language Summary In addition to regional monsoon systems, the Southeast Asian climate is largely controlled by the South China Sea (SCS) and adjoining seas, which are linked through several straits and passages. The physics controlling the movement of water and heat through these oceanic pathways are thus key to this region and beyond. The absence of consistent and long-term ocean observations in this region poses challenges to understanding these physics. Due to the presence of many small islands, high-resolution model experiments are essential to resolve the ocean circulations in the Southeast Asia region. Here, using a high-resolution *regional* ocean model simulation, we characterize the unique seasonal structure of transports through six straits in the SCS in terms of regional drivers. Further, we investigate a deep water mass in the Luzon Strait and identified its origin in the central Pacific Ocean. Lastly, using high-resolution *global* climate model simulations we show projected changes in upper ocean behavior in the SCS and maritime continent at the end of the 21st century assuming continued high greenhouse gas emissions, particularly the net heat convergence in the SCS and reduction in the upper ocean mixing. These projected changes have the potential to modulate the ocean-atmosphere interactions and climate globally.

1. Introduction

The South China Sea (SCS) is the largest semi-enclosed marginal sea in the tropics with several passages linking to neighboring oceans. It is surrounded by a steep continental slope and linked with the western Pacific Ocean through the Luzon Strait, to the Sulu Sea through the Mindoro Strait, to the Java Sea through the Karimata Sea, and to the East China Sea through the Taiwan Strait (see Figure 1). Due to its unique location and bathymetry, the SCS has the characteristics of both shelf seas and tropical oceans. While the

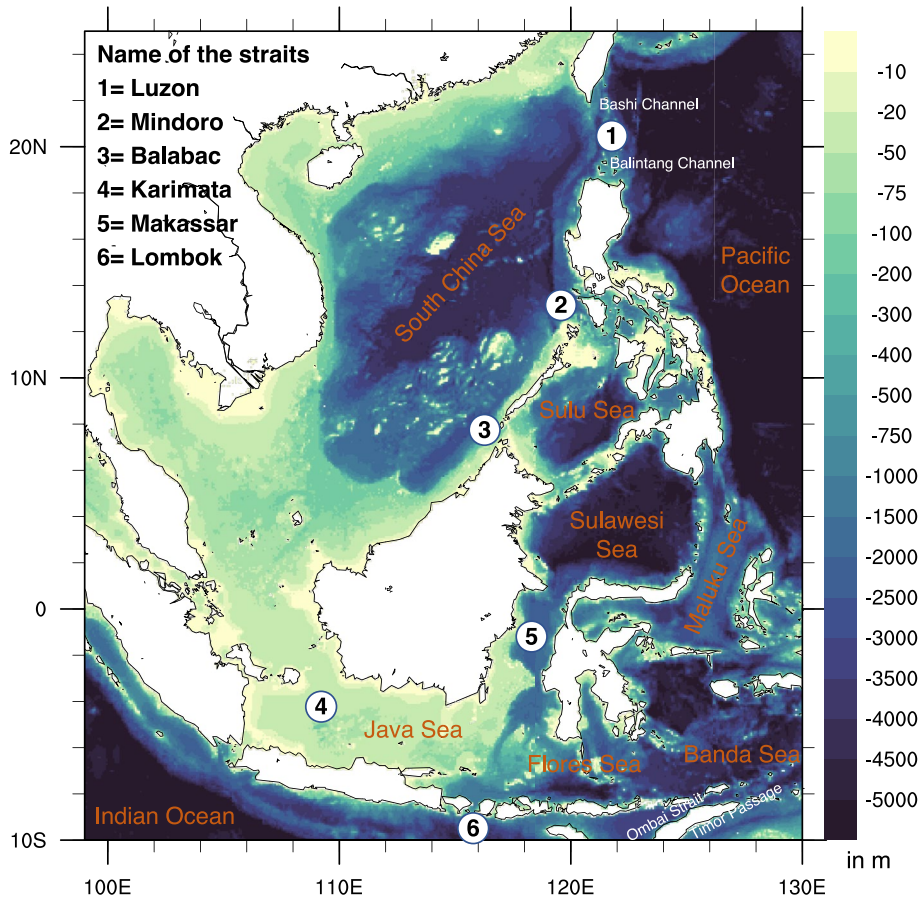

Figure 1. Regional ocean modelling system (ROMS) domain and bathymetry from ETOPO1 (in m). Straits examined in detail in this study are numbered.

Luzon Strait plays a major role in transport between the tropical Pacific and SCS (Deng et al., 2018; Qu et al., 2004; Wyrtki, 1961), other surrounding straits have significant control on the SCS climate as well. Understanding monsoon modulated SCS transports are critical for a multitude of factors such as upper ocean dynamics over the SCS (e.g., Liu et al., 2008), interaction with the western tropical Pacific Ocean (e.g., Xue et al., 2004), and Indonesian throughflow (ITF) (e.g., Tozuka et al., 2007, 2009). These factors in turn can modulate regional air-sea interactions and climate. Furthermore, as the ITF is an important conduit of the global thermohaline circulation, understanding transports across the maritime continent (MC) has global climatic relevance.

As anthropogenic warming continues, the world ocean absorbs excess heat. During 1971–2010 about 64% of this excess heat is stored in the upper 700 m (93% for full depth) (Pörtner et al., 2019). With the continued warming rate up to the end of the 21st century, upper ocean dynamics and marine biogeochemistry are projected to change, potentially beyond the current range of mean and variabilities in different timescales (e.g., Fasullo et al., 2020; Kwiatkowski et al., 2020; Qu et al., 2019; Silvy et al., 2020; Toste et al., 2019). It has also critical consequences for regional ocean dynamics and rising sea levels. These are particularly concerning over the SCS and MC due to the presence of many low-lying islands. The livelihood of highly populated, low-income countries of this region is dependent on the ocean (e.g., Ferrol-Schulte et al., 2015; Gamage, 2016; Zhang, 2018). However, the future changes in local and regional characteristics of the SCS, including mass and heat transport, and upper ocean behavior (such as heat content, salinity, and mixed layer depth [MLD]) are poorly understood. Regardless of which socio-economic pathways (SSP) becomes the reality at the end of the 21st century, we must understand the regional upper-ocean changes under the high emission scenario.

Our ability to understand upper ocean characteristics largely relies on ocean observations. There has been a significant advancement in world ocean observations, however, the SCS and MC remain data sparse. Despite many efforts to deploy floats to contribute to the Argo network, Argo profile density over the SCS and MC remains notably less than other oceans. This is due to a lack of consistent long-term floats and operational constraints over shallow regions (see Figure S1). Any recent map shows the absence of Argo profiles in the SCS and MC (Figure S1c). Consequently, observational studies over the SCS and MC are limited to short-term floats (e.g., Zhou et al., 2010) and different field campaigns (e.g., International Nusantara Stratification and Transport program (INSTANT); Gordon et al., 2008, 2010, World Ocean Circulation Experiment) over the region. Efforts also have been made to generate observational databases such as the international quality-controlled ocean database, World Ocean Database (WOD), IFREMER MLD climatology at 2° resolution (de Boyer Montégut et al., 2004), and SCS physical oceanography datasets at 0.5° resolution (SCSPOD14, Zeng, et al., 2016), for particularly SCS. However, these remain insufficient due to either lack of coverage or lower spatial resolution.

Since Wyrtki (1961), dozens of studies have focused on Luzon Strait transport based on short-term (<two months) observational campaigns (e.g., Guo & Fang, 1988; Liao et al., 2008; Tian et al., 2006; Xu et al., 2007; Xu, 2004; Yuan et al., 2012; Yuan et al., 2014; Zhou et al., 2009) and long-term (multi-year) campaigns (Chu & Li, 2000; Jian et al., 2004; Nan et al., 2013; Qu, 2000; Wang et al., 2006). Most of these studies suggest the net water inflow from the western Pacific Ocean to SCS, however, monsoon-induced strong seasonality is notable. Such estimates of Luzon Strait transport are limited to the upper few hundred meters of the ocean. On the other hand, quantitative knowledge of ITF behavior relies on many short-term to few years of field campaigns, such as over Mindoro Strait (Gordon et al., 2011), Makassar Strait (Ffield et al., 2000; Gordon et al., 1999, 2010, 2019; Susanto & Gordon, 2005; Susanto et al., 2012), Karimata Strait (Fang et al., 2010; Susanto et al., 2013, 2016; Wang et al., 2019; Wei et al., 2019; Xu et al., 2021), and Lombok Strait (Sprintall et al., 2009).

Past efforts also include understanding transport through the SCS and surrounding seas from paleoclimate reconstructions. For example, Luzon Strait transport was reconstructed from a 68-year long, annually resolved coral radiocarbon record (Ramos et al., 2019). Centennial changes to Holocene Makassar Strait transport and ITF transport were reconstructed from sediment cores (Fan et al., 2013; Linsley et al., 2010). Finally, a multi-proxy approach was used to reconstruct ITF transport since the last glacial maximum (Ding et al., 2013).

These datasets provide an important background of past transports and ocean behavior over this region. However, there are several limitations in studying spatio-temporal variability of upper ocean behavior over the SCS region with these datasets, such as large data gaps over the region, coarse horizontal resolution, discontinuous time series, lack of longer records, and surface-only datasets. Moreover, most observations rely on hydrographic data and are dependent on the assumption of geostrophy. The above-mentioned observational datasets pose a challenge in understanding the spatio-temporal structure of transports and upper ocean behavior due to the presence of many small islands and largely varying bathymetry (~5–5,000 m) in this region.

While all these observational studies are point-based and limited to several hundred meters of the upper ocean, numerical model simulations estimate the full, time-varying structure of the ocean. Previous studies examined ocean behavior and transports over the SCS, mainly the Luzon transports using ocean general circulation models; for example, using the Naval Research Laboratory Layered Ocean Model at 0.5° (Metzger & Hurlburt, 1996), the Parallel Ocean Climate Model based on the Bryan-Cox model at 0.4° (Wajsowicz, 1999), the Miami Isopycnic Coordinate Ocean Model at 1/4° (Liang et al., 2008), and the quasi-global HYbrid Coordinate Ocean Model at ¼-2° resolution (Wang et al., 2009). However, it remains challenging to study the local features of the SCS or transport using these global models due to their coarser horizontal resolution and typical mean-state biases (e.g., Samanta et al., 2018, 2019); which is in turn related to the horizontal resolution to a large extent. These suggest the need for regional ocean model studies. Consequently, there are several regional ocean model-based simulations to study SCS dynamics and Luzon transport, such as, with Modular Ocean Model version-2 at 1/4° (Qu et al., 2004), and Princeton Ocean Model at ¼-2° (Hsin et al., 2012; Wei et al., 2009). Of late, with the availability of better computing resources, higher resolution

regional model studies have also been initiated over SCS (Fang et al., 2005; Jiang et al., 2020; Li et al., 2019; Liang et al., 2019; Liu & Gan, 2017; Nan et al., 2013).

However, all these studies are either focused on a short period of simulation, the northern SCS (e.g., Jilan, 2004), SCS-averaged layer circulation (e.g., Gan et al., 2016), the ITF region, the Kuroshio region, or different aspects of SCS that are unrelated to SCS transport. Consequently, regional and local drivers determining the vertical structure of various straits in the SCS and MC have received less attention. While the Luzon Strait remains the primary focus of most studies, it is also important to understand the ocean behavior of the other straits surrounding the SCS and MC. Using four years of regional model simulations, Li et al. (2019) investigated the impact of the closing of Luzon, Sibutu, and Karimata Straits on the upper 300 m within the SCS and the ITF over the almost similar domain as ours. However, understanding seasonal climatological variations in the vertical structure across these straits and upper-ocean mixing processes are important and remain less studied. It can unfold the driving forces for transports and their responses. We also know a little about the seasonal variability of deeper water masses around the Luzon Strait. Limited measurements inferred recent changes in the ITF region due to changes in Indo-Pacific wind and buoyancy forcing (Sprintall et al., 2019). However, future projections of regional ocean behavior and transport across the SCS and MC are rare. Further, the typical coarse resolution (~1°) of the ocean component of the global climate model simulations from Coupled Model Intercomparison Project (CMIP) Phase 5 (CMIP5) or Phase 6 (CMIP6) is not sufficient to study future projection of local and regional ocean behavior across the SCS and its transports due to presence of many small islands, narrow straits, and passages.

Identifying these research gaps, we aim to synthesize the existing views of climatological SCS transport and add new knowledge to its seasonal ocean behavior in the entire SCS and MC that comprise many straits and passages (Figure 1). Further, we explore the seasonal changes in mass and heat transport and related upper ocean behavior over this region (Figure 1) by the end of the 21st century.

We set three objectives for our study: (a) characterizing the structure of transport through straits in the SCS and MC in terms of regional drivers, (b) examining the seasonal variability of deepwater masses across the Luzon Strait, and (c) exploring the projected changes in transport and upper-ocean behavior over the SCS and MC region by the end of 21st century under the high-emission scenario. For the first and second objectives, we use the regional ocean modelling system (ROMS), whereas High-Resolution Model Intercomparison Project (HighResMIP, Haarsma et al., 2016) simulations are exploited for the third objective. We focus on six straits, namely, Luzon, Mindoro, Balabac, Karimata, Makassar, and Lombok (see Figure 1).

2. Data and Models

2.1. Observations

The study domain (Figure 1) covers the SCS and MC. It is situated within a complex terrain with widely varying bathymetry. ROMS simulations were validated using several observational datasets at monthly resolution: Sea surface temperature (SST) data from NOAA optimally interpolated SST version 2 (OI; 0.25° × 0.25° resolution; Reynolds et al., 2002); sea surface salinity (SSS), and MLD (based on temperature criteria) from SODA version 3.3.1 reanalysis (0.50° × 0.50° resolution; Jackett et al., 2006) and SCSPOD14 data (0.50° × 0.50° resolution; Zeng et al., 2016). SCSPOD14 consists of validated Argo floats, in situ observations from World Ocean Atlas 2009 (WOA09), and South China Sea Institute of Oceanography measurements for 1919–2014. Additionally, we used monthly climatological products from JAMSTEC Grid Point Value of the Monthly Objective Analysis using the Argo data (MOAA GPV; Hosoda et al., 2008) at 1.0° × 1.0° resolution. MOAA GPV is a gridded quality-controlled data combining Argo float, Triangle Trans Ocean Buoy Network (TRITON) mooring, and available shipboard conductivity, temperature, and depth (CTD) device since 2001. For estimating density values for the temperature-salinity (T-S) diagram, the CSIRO seawater package http://www.cmar.csiro.au/datacentre/ext_docs/seawater.htm) is used. Surface net heat flux data is used from WHOI OA flux products (1.0° × 1.0°; Yu et al., 2008).

2.2. ROMS

ROMS is a free-surface, three-dimensional, terrain-following, primitive equation ocean model (Shchepetkin & McWilliams, 2003, 2005) and widely used by the scientific community for a diverse range of applications over different regions (e.g., Blanke et al., 2002; Dey et al., 2020; Haidvogel et al., 2000; Liu et al., 2016; Peliz et al., 2003), including the SCS (Fan et al., 2014). ROMS solves the hydrostatic primitive equations for momentum using a split-explicit time-stepping scheme that requires coupling between barotropic (fast) and baroclinic (slow) modes. We used the ROMS Agrif version 3.1.1 distribution over the domain covering 10°S–25°N, 99°E–130°E (see Figure 1) with an average horizontal resolution of 1/5° (approximately 22 km with 181 (longitude) × 156 (latitude) grid points) with 32 vertical levels structured on a sigma coordinate scheme. All the boundaries were kept open and tides were included for the simulation. The initial and lateral boundary conditions were derived from the climatological fields of WOA09, Levitus et al., 2010). Monthly varying climatological forcing fields consisting of wind stress, air temperature, relative humidity, specific humidity, air density, air-sea fluxes, evaporation, and precipitation fluxes were taken from monthly climatology of the Comprehensive Ocean-Atmosphere Data set (COADS; Da Silva et al., 1994). These forcing fields of the horizontal resolution of 0.5° × 0.5° were linearly interpolated to the model grid. We used the K-profile parameterization (KPP) scheme (Large et al., 1994) for the vertical mixing scheme in the simulation and included bulk flux computation for surface fluxes to avoid heat flux adjustment and relaxing model SST toward observed values. The maximum value of the slope parameter 'r' was set to 0.25 for topography smoothing. For a better simulation of upper ocean behavior, the vertical resolution was enhanced toward the surface. The ROMS was spun up from the rest and run for 22 years. We obtained three-day output and present seasonal climatological features of the last 15-year run.

2.3. CMIP6 HighResMIP

To study the future projections, we used model output from the HighResMIP project, which is a subset of models under CMIP6 with a high spatial resolution (Haarsma et al., 2016). The forcings used in HighResMIP runs are identical to those of CMIP6; see Eyring et al. (2016) for details. As capturing regional climate variability and change relies on the ability to resolve the driving processes, HighResMIP enables assessments of the impact of increased horizontal resolution in coupled climate model simulations.

We used HighResMIP monthly outputs from historical (1850–2014) and future projection (2015–2100) simulations, where the latter were driven by forcings associated with the SSP5-585 scenario. The SSP5-585 scenario is roughly equivalent (but not identical) to the Representative Concentration Pathway 8.5 (i.e., RCP8.5) scenario in earlier CMIPs. As SSP5-585 is associated with the highest emission scenario in CMIP6, future changes can expose the changes arising from the forced response. The models were selected based on the availability of the following variables for both historical and SSP5-585 scenarios with the same ensemble member (with same realization, initialization, and model physics): zonal and meridional component of mass transport, vertically integrated heat transport, upper 300 m averaged heat content (HCONT300), sea surface salinity (SSS), and mixed layer depth (MLD). Three HighResMIP models met these criteria: CNRM-CM6-1-HR (Voldoire et al., 2019), HadGEM3-GC31-MM (Williams et al., 2018), and MPI-ESM1-2-HR (Gutjahr et al., 2019). Here we show the multimodel ensemble results throughout. The details of the models used are listed in Table S1. The mass transport components are from residual mean (resolved plus parameterized) advective transport. The heat transport components contain contributions from resolved and parameterized processes.

We present seasonal climatological results for summer (JJA), and winter (DJF) consistently, unless otherwise stated. After examining the consistent match of climatological features from HighResMIP with observations (climatology is shown in Figure S9) we explore the future changes. While showing the future changes using HighResMIP, the model biases are removed to the extent possible as we show the climatological difference between the two periods. The horizontal resolution of the ROMS simulation is higher than HighResMIP, but conducting interannual simulations for 1850–2100 or running such global climate models with further higher resolution is computationally expensive. Therefore, we adopted this hybrid approach to examine the past, present, and future, allowing reflection on future ROMS experiment designs by gaining knowledge of future changes from HighResMIP simulations.

All the above data sets (observations/reanalysis, ROMS outputs, and HighResMIP archive) are freely and publicly available online; see Data Availability Statement.

2.4. Site Selection

We study ocean transports of the six straits within the domain: Luzon, Mindoro, Balabac, Karimata, Makassar, and Lombok (Figure 1). The selection of these straits is not random, rather based on the assessment of whether or not ROMS and HighResMIP model grids can resolve the width of the straits. The minimum width of the Luzon Strait (~360 km), Mindoro Strait (~84 km), Balabac Strait (~46 km), Makassar Strait (~117 km), Karimata Strait (~324 km), and Lombok Strait (~36 km) are resolved by ROMS and HighResMIP grids. For the same reasons several other water channels in the domain (e.g., Ombai Strait, Timor Passage) are not examined.

3. Results and Discussion

3.1. Evaluation of ROMS Climatology

We use SST, SSS, and MLD to evaluate ROMS's capability in simulating seasonally varying upper ocean behavior over the domain. SST is strongly related to upper ocean heat content and is important for upwelling, ocean currents, and air-sea fluxes. SSS is an essential climate variable which plays a critical role in density-driven ocean circulation, the water cycle, and climate; whereas MLD is the manifestation of turbulent mixing processes. SST, SSS, and MLD (Figure 2) show strong seasonal variability over the SCS. During summer (JJA), SST over the entire basin north of the equator is greater than 28.5°C, whereas, in winter, a strong SST gradient parallel to the coast is seen over the northern and western SCS. SST over the ITF region is rather uniform in winter. All these features are reasonably well simulated in our ROMS simulation compared to observations (OBS). Seasonal SSS variability is also consistent with the reanalysis data (Figures 2e–2h). Seasonally varying MLD patterns are simulated to a large extent, including the northeastern part of the domain over the western Pacific where MLD has a strong seasonal variation (Figure 2i–2l). The observed MLD mismatch between ROMS and reanalysis is due to different calculation criteria. While SODA MLD is calculated from temperature profiles, ROMS MLD is determined by the KPP mixing scheme. The mismatch in these variables near the Mekong river delta and Yangtze river maybe also due to the exclusion of river discharge in the ROMS simulation. However, in line with our approach, earlier regional modeling studies found that exclusion of river input does not significantly affect large-scale, seasonally varying patterns of SST, SSS, sea surface height, circulation, and transport in the SCS (e.g., Chu et al., 1999). The overall match of ROMS SSS is significant because the model is prescribed with observations. While comparing SST, SSS, and MLD with observation-based SCSPOD14 data over the SCS, we also found our ROMS setup simulates seasonal climatological patterns reasonably well (Figure S2).

We further validate ROMS simulations for net heat flux and vertical profiles over the domain. ROMS setup is quite well capable of simulating seasonal climatological net heat flux, including a striking north-south dipole pattern in the winter (Figure S3). Vertical structure of annual climatology of temperature and salinity across the Luzon Strait (18°N, also shows a reasonable match with observations (Figure S4 and Figures 9a–9d of Zeng et al., 2016) with a downward slope east of 115°E. Next, we utilize the location of the INSTANT field campaign (Gordon et al., 2008) to assess the meridional velocity profile in Makassar Strait. ROMS vertical profile shows a reasonable agreement with the observations including peak southward velocity around 150 m depth (Figure S5). We also find reasonable matches in vertical profiles in other locations in our study domain including the Luzon Strait. Lastly, we assess water mass characteristics (in terms of annual mean T-S scatter diagrams averaged over 5° × 5° subareas within our domain (Figure S6), which reflects a reasonable consistency with observational datasets of SCSPOD14 (Zeng et al., 2016).

Such reasonably consistent climatological features of the upper ocean in the SCS allow us to delve deeper into the simulated transports through the straits of the SCS and MC from the ROMS simulations.

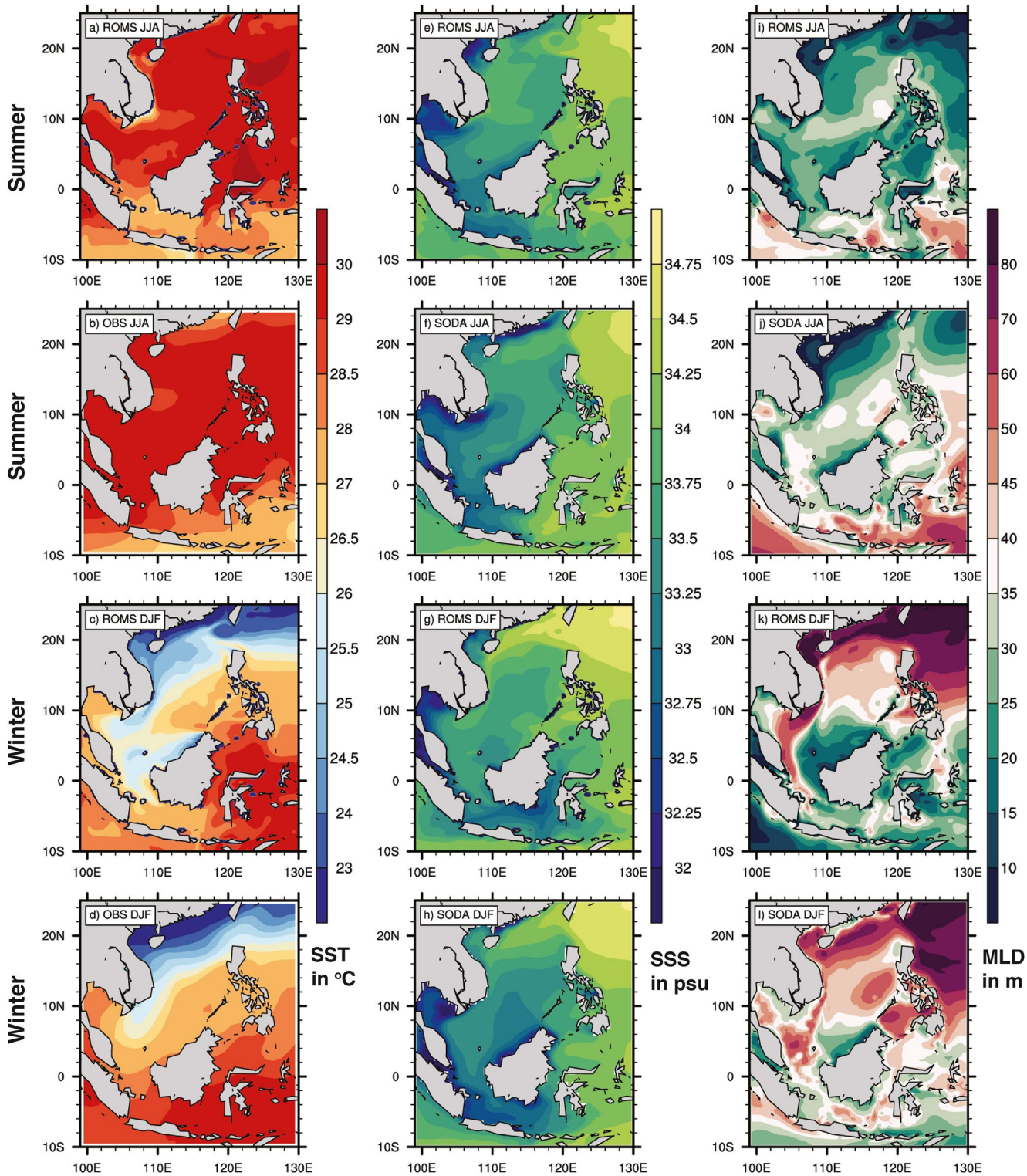

Figure 2. Comparison of seasonal climatological features of upper-ocean between regional ocean modelling system (ROMS) and observations/reanalysis (OBS). Seasonal climatologies for (a–d) sea surface temperature (SST; in °C), (e–h) sea surface salinity (SSS; in psu), and (i–l) mixed layer depth (MLD; in m). The OBS SST is from OISST, whereas, SSS and MLD are from SODA. Summers and winters are indicated by JJA and DJF, respectively.

3.2. Simulated Transports Through Different Straits

After originating from the North Equatorial Current (NEC), the Kuroshio Current plays an important role in mass and heat transport to the western Pacific warm pool and SCS via the Luzon Strait (Nan et al., 2015). While passing by the Luzon Strait, a branch of the Kuroshio flows into SCS through the Balingtang channel, and a large portion of Kuroshio water flows out of the SCS via the Bashi channel (e.g., Nan et al., 2015; Qu & Lukas, 2003; Zhai & Hu, 2013). Despite considerable seasonal changes, we found the total westward transport through Luzon Strait is consistent with earlier studies (e.g., Nan et al., 2015). The vertically integrated Luzon Strait transport (Figures 3a and 3b) is −7.5 Sv in summer and −11.2 Sv in winter. These are consistent with earlier estimates from observations, models, and paleo reconstructions (e.g., Ramos et al., 2019; Qu et al., 2004; Wei et al., 2009). Observations and models agree with our results (Figures 3a and 3b) that total Luzon Strait transport is essentially westward, that is, from the tropical Pacific to SCS. The westward flow is largely due to the strong diapycnal mixing in the Luzon Strait, which maintains the baroclinic pressure gradient across the Luzon Strait driving the Luzon overflow (Wang et al., 2017; Zhao et al., 2014) and deep SCS upwellings (Qu, Girton, & Whitehead, 2006). Using a modeling study, Song (2006) showed a westward transport of 8.2 Sv in summer and 12.2 Sv in winter, which is also consistent with our ROMS simulation. However, a large range of estimates across studies is due to the differences in the methodology including model diversity (Hsin et al., 2012; Nan et al., 2015).

Observational estimates reveal considerable seasonal-to-interannual variations in ITF transport (Gordon, 2005; Gordon et al., 2010; Pujiana et al., 2009; Sprintall et al., 2000; Susanto et al., 2000; Wijffels et al., 2008). The Makassar Strait is the western-most deep channel of the ITF and encompasses about ∼80% of southward ITF transport (Gordon et al., 2010; Lee et al., 2019) with ∼4.5 Sv in winter and 12.1 Sv in summer (Figures 3a and 3b). It is noteworthy that higher Makassar Strait transport values (than our simulation) in earlier field campaigns are mostly due to their observational locations toward the east of the strait where velocity is higher (e.g., INSTANT observations at 2.5°S). Compared to the Luzon and Makassar Straits, the seasonal mean transports across the Mindoro and Balabac Straits are much weaker (Figures 3a and 3b). Whereas, the Karimata Strait transport is strongly driven by seasonally varying monsoon winds over the region, therefore, has strong seasonality in the transport. Our simulations also indicate transport direction and magnitude vary depending on the location in the Karimata Strait. Volume transport through the Karimata Strait varies between 4 Sv in winter to 1.5 Sv in summer, which is consistent with the recent findings of Xu et al. (2021). For the Lombok Strait, the transport is southward, increasing in winter (relative to summer) under the influence of stronger Makassar and Karimata Strait transport (Figures 3a and 3b; Gordon, 2005; Gordon et al., 2010).

We further explore the vertically averaged zonal and meridional momentum transport over the domain in summer and winter (Figures 3c–3f). During summer, strong eastward zonal transport is simulated in the upper northern Luzon Strait (up to 0.4 m/s), the Vietnam upwelling region, and the southern part of the Karimata Strait. In winter, the eastward zonal flow becomes very pronounced in the Karimata Strait, reduced over the northern Luzon Strait, and reversed over the Vietnam upwelling region following a wind reversal. In contrast, stronger (weaker) southward meridional flows are observed during winter (summer) over the Vietnam coast, and Taiwan, Makassar, and Lombok Straits.

3.3. Vertical Structure Across Different Straits

The water column structure across the six straits is investigated to improve our understanding of verticle stratification and mixing. We carefully selected the cross-sections to align as well as possible with the previously mentioned observational studies.

The Luzon Strait is the widest (∼360 km) and deepest (∼2.5 km) among all the SCS and MC straits; we examine the vertical distribution of water properties and transports along 120.8°E for summer (JJA), and winter (DJF) (Figure 4). The simulated distribution of zonal velocity in this cross-section suggests that Luzon transport is limited to the ∼upper 500 m in the south, and is surface-intensified but extends gradually to the bottom in the north, which is consistent with earlier findings despite the little diversity in the vertical extension of the transport in different numerical modeling studies (Qu, 2002; Qu et al., 2004). The striking dipole-like pattern in zonal velocity (Figures 4a and 4b) with the westward flow (inflow to the SCS) in the

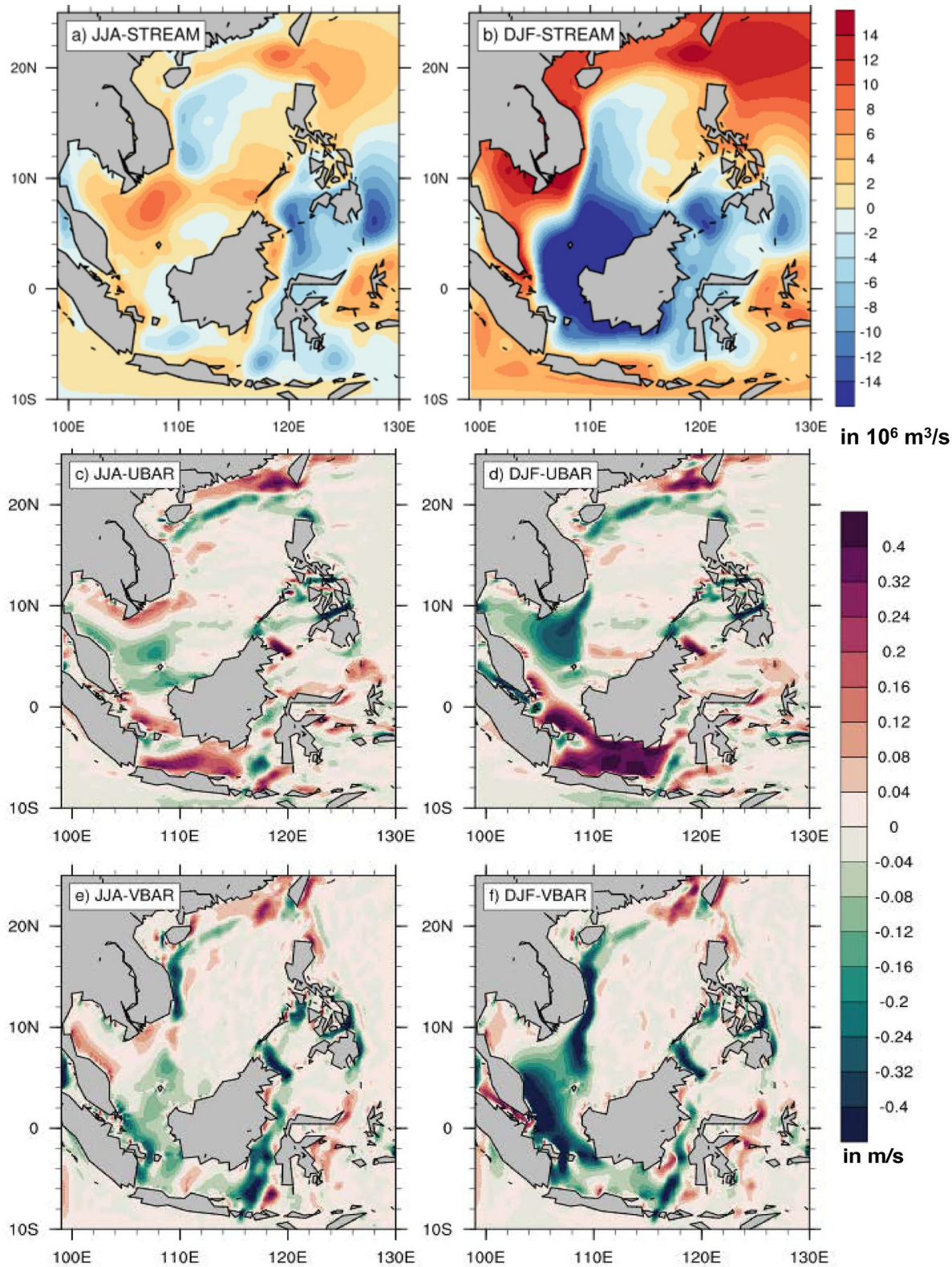

Figure 3. Seasonal climatology of vertically integrated volume and average momentum transport from regional ocean modelling system (ROMS) simulation (a and b) vertically integrated volume transport (stream function; in 10^6 m^3/s), (c and d) zonal momentum transport (in m/s), and (e and f) meridional momentum transport (in m/s) over SCS. Summer (JJA) and winter (DJF) are shown in the left and right panel, respectively.

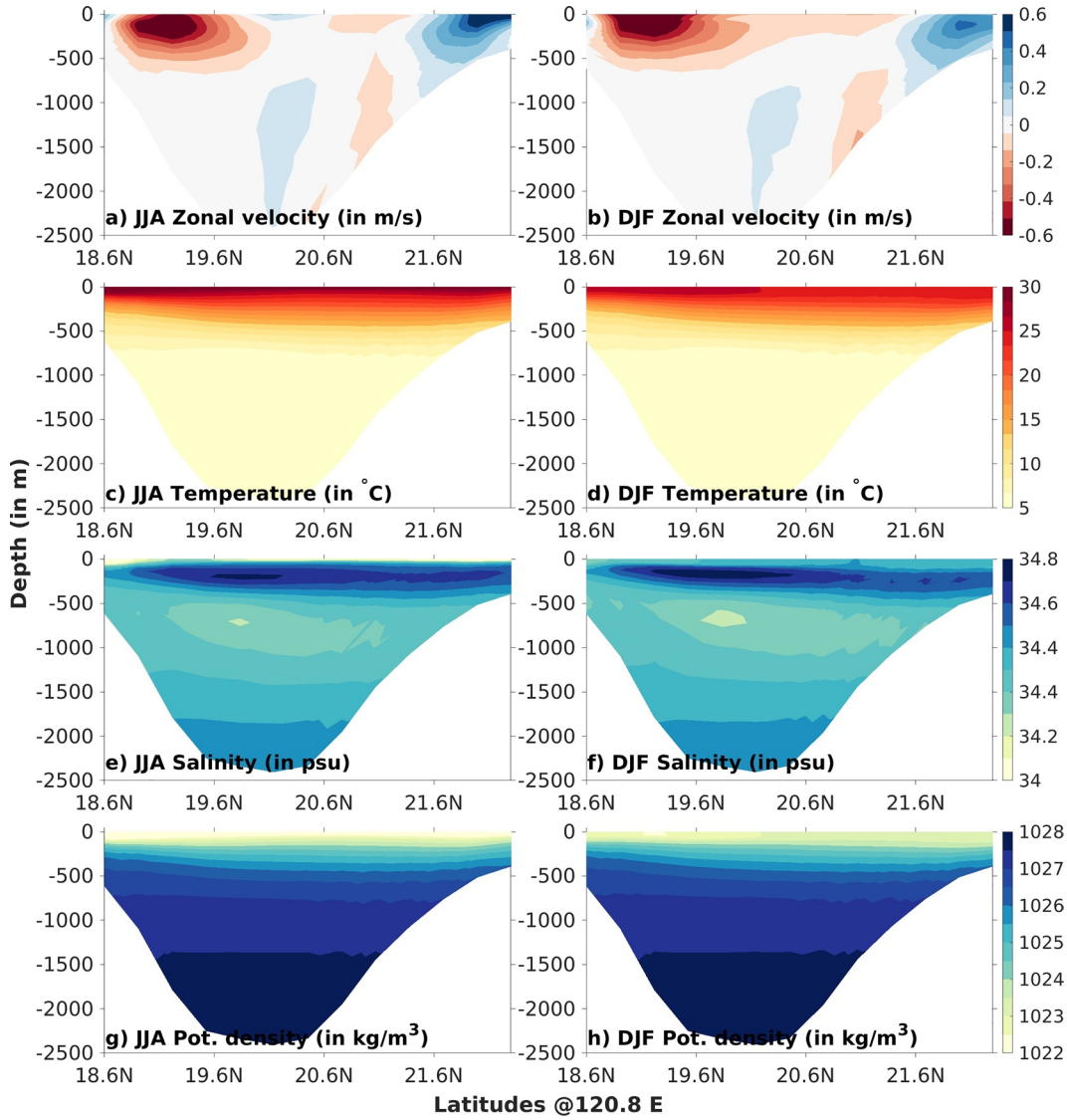

Figure 4. Seasonal climatological vertical structure of Luzon Strait at 120.8°E from regional ocean modelling system (ROMS) simulation. Climatology of (a and b) zonal velocity (in m/s), (c and d) temperature (in °C), (e and f) salinity (in psu), and (g–h) potential density (kg/m^3). Summer (JJA) and winter (DJF) seasons are shown in the left and right panel, respectively.

south and eastward flow (outflow) in the north of the Luzon Strait is evident. The inflow is stronger and wider (up to 0.6 m/s) than the outflow (up to 0.4 m/s) (Figures 4a and 4b), indicating the net westward inflow to the SCS. During the winter, inflow increases, and outflow decreases (Figure 4b), thereby, the net inflow increases to the SCS than in the summer. A seasonally invariant weak outflow from the SCS at 19.8°N and 20.6°N and inflow around 20.9°N is also noted. This sheared vertical structure (i.e., inflow in the upper layer accompanied by outflow in the intermediate layer) is more pronounced in winter at approximately 20°N. This sheared vertical structure is somewhat similar to a few earlier studies investigating the annual structure of the Luzon Strait (e.g., Jiang et al., 2020; Qu, 2002), however three-layer structure along the cross-section (e.g., Zhu et al., 2019) is not pronounced. The Kuroshio intrusion enters the SCS carrying warmer and saltier water from the western Pacific Ocean (e.g., Nan et al., 2015**).** As the outflow velocity through Luzon Strait is weaker, there is an exchange of water and nutrients along the strait (Figure 4; Qu et al., 2004). Luzon Strait temperature structure shows a cooling up to 2°C (toward the northern side) in winter from summer (Figures 4c and 4d), however, seasonal temperature changes in the deep layers are relatively much less. The salinity structure (Figures 4e and 4f) shows the occurrence of stratification and the

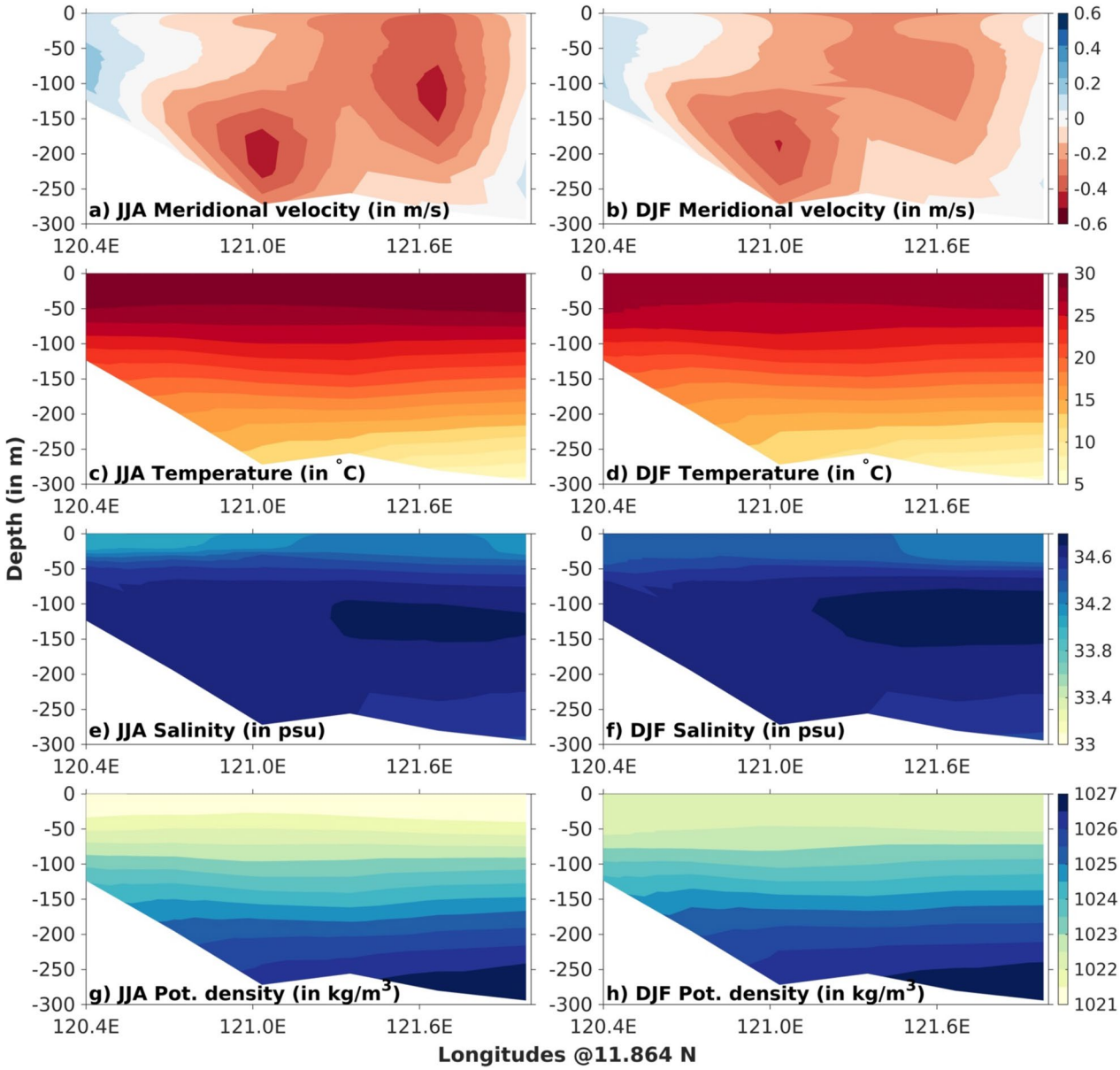

Figure 5. Seasonal climatological vertical structure of Mindoro Strait at 11.864°E from regional ocean modelling system (ROMS) simulation. Climatology of (a and b) meridional velocity (in m/s), (c and d) temperature (in °C), (e and f) salinity (in psu), and (g and h) potential density (kg/m^3). Summer (JJA) and winter (DJF) seasons are shown in the left and right panel, respectively.

formation of a barrier layer. The absence of pronounced seasonal changes in intermediate and deepwater salinity is associated with the presence of thicker (thinner) low-saline water at the surface and high-saline water in the sub-surface during the summer (winter) (Figures 4e and 4f). The density distribution (Figures 4g and 4h) reflects the salinity structure, however, summer freshening (up to 1,022 kg/m^3) in the upper 100 m relative to winter is noticeable.

While moving south in the domain, Mindoro Strait connects the SCS to the Sulu Sea. Net southward flow through the Mindoro Strait is stronger and deeper in summer relative to winter (Figures 5a and 5b), with peak velocity centered around 121°E and 121.6°E. The seasonal variation of velocity variation and magnitude ~250 m in ROMS simulation (Figures 5a and 5b) is consistent with Gordon et al. (2011)'s observation. During summer the upper 60 m shows the presence of warmer (>27°C), fresher (<33.6 psu), and less dense (<1022 kg/m^3) water than in winter. These notable seasonal changes are more pronounced in the western

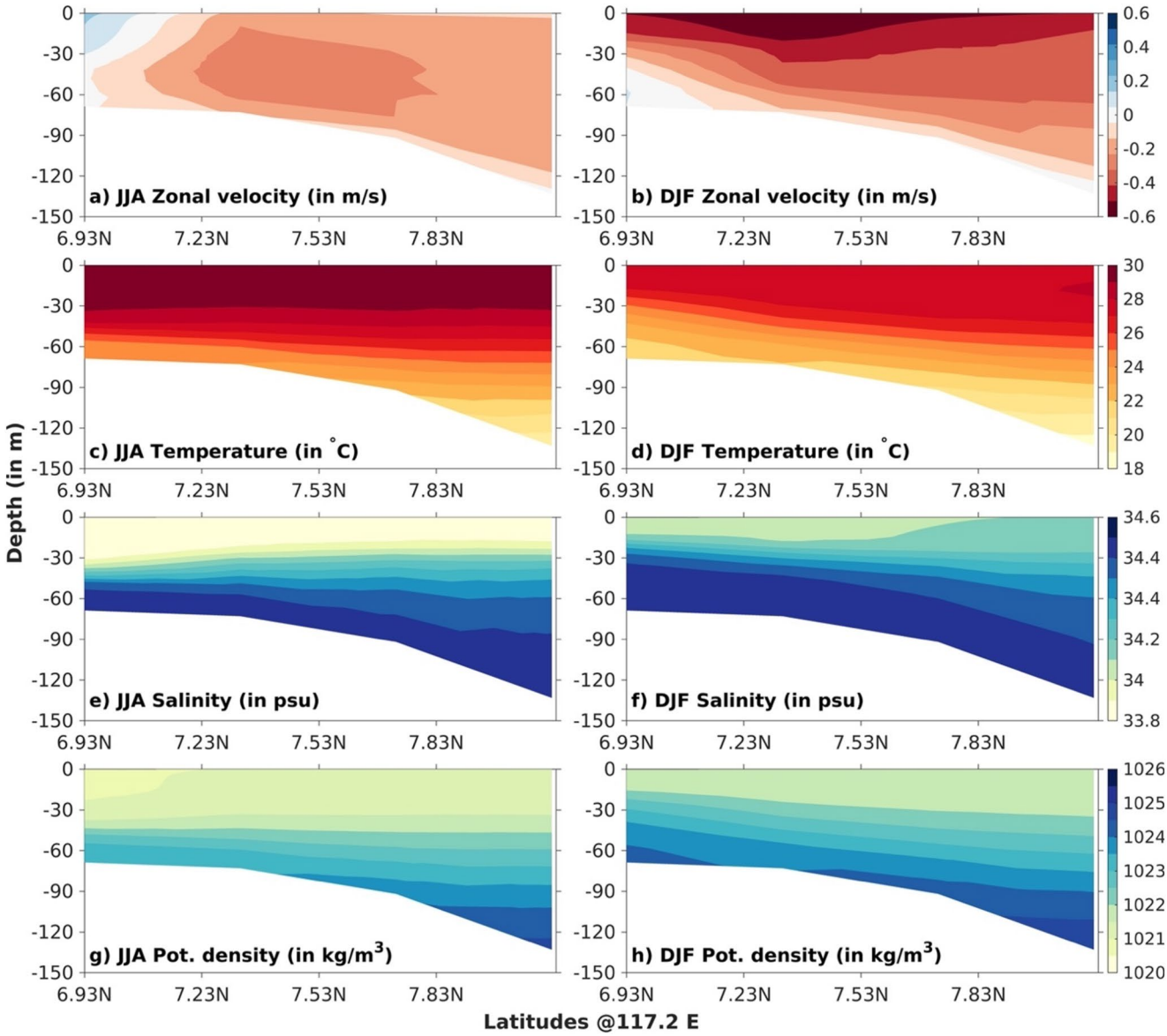

Figure 6. Seasonal climatological vertical structure of Balabac Strait at 117.2°E from regional ocean modelling system (ROMS) simulation. Climatology of (a and b) zonal velocity (in m/s), (c and d) temperature (in °C), (e and f) salinity (in psu), and (g and h) potential density (kg/m^3). Summer (JJA) and winter (DJF) seasons are shown in the left and right panel, respectively.

part of the strait, where a seasonally invariant weak northward flow up to 150 m is noted. However, we do not notice any pronounced barrier layer in the Mindoro Strait (Figures 5d–5f).

To the south, the Blabac Sea is another connector between the SCS and the Sulu Sea. It is deeper along the north with depths ranging from ~65 m in the south to ~140 m in the north. Balabac Strait shows a notable seasonality. The surface layer during the winter season displays an increased westward flow up to 0.6 m/s than maximum summer westward velocity of 0.2 m/s (Figures 6a and 6b), and up to 4°C cooling than summer. It is associated with the presence of less saline (~0.6 psu less than summer), and lighter water mass (Figures 6e–6h). However, the subsurface structure of the Balabac Strait is quite homogeneous, independent of seasonality, and free from barrier layer formation (Figure 6).

Moving farther southward in the domain we encounter the Makassar Strait that connects the Sulawesi Sea with the Java Sea. As low-saline, buoyant surface water from the SCS enters the Makassar Strait, it restricts the Mindoro current surface water into the Makassar Strait (Gordon et al., 2012). The average thermocline

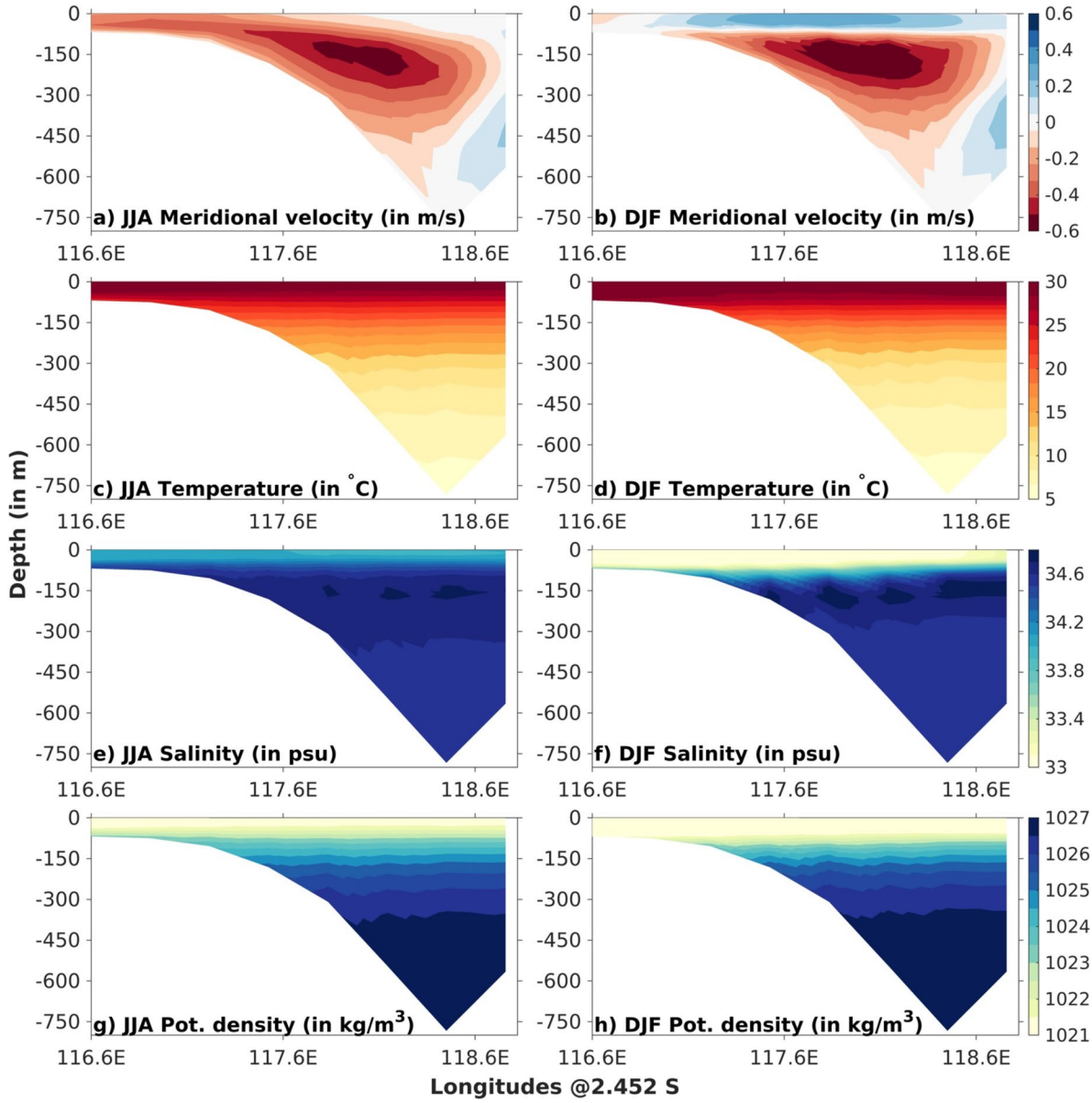

Figure 7. Seasonal climatological vertical structure of Makassar Strait at 2.452°S from regional ocean modelling system (ROMS) simulation. Climatology of (a and b) meridional velocity (in m/s), (c and) temperature (in °C), (e and f) salinity (in psu), and (g and h) potential density (kg/m^3). Summer (JJA) and winter (DJF) seasons are shown in the left and right panel, respectively.

layer in the Makassar Strait is 50–200 m with a vertical temperature gradient of 0.31°C/10 m (Gordon et al., 2012). Our knowledge of the vertical structure in the Makassar Strait is primarily based on multiple studies based on INSTANT (Gordon et al., 2008, 2010; Susanto et al., 2012) and ITF recovery experiments at Labani Channel (MITF; e.g., Gordon et al., 2019). Meridional velocity at the Labani channel (~2.5°S) reaches its maximum southward velocity around 150–200 m and subsequently decreases to a near-zero value around 800 m depth. Our ROMS simulation simulates this feature of INSTANT location reasonably well, however, a subsurface positive bias (~25 m depth) exists (Figure S4). The seasonally invariant southward flow of the ITF through the Makassar Strait is seen throughout the strait (Figures 7a and 7b). The maximum southward flow is observed between 117.8°E and 118.4°E around 110–250 m. Consistent with earlier studies, the results show an increase in southward flow (~0.6 m/s) in winter than in summer. The upper 50 m in winter also shows a weak northward flow. The strongest mean velocity ~0.6 m/s is consistent with earlier reported 16-month mooring observations (e.g., Gordon & Susanto, 1998). As summer progresses to winter,

the maximum temperature reaches a deeper layer ~75 m relative to ~50 m in summer. However, subsurface and deep layer temperature show little seasonality (Figures 7c and 7d). The salinity and density structure show a strong seasonality in the Makassar Strait, comprising a fresher (and lighter) layer in the winter than in the summer. The winter salinity in the upper 70 m remains ~33–33.2 psu. The presence of such a fresh layer in the winter may be related to anomalous positive net heat flux (Figure S3) around the region.

Karimata Strait acts as not only an outflow strait of the SCS throughflow but also the inflow strait of the ITF. Karimata Strait is the shallowest within our study domain and has a uniform depth of ~70 m. Generally, the annual cycle of Makassar Strait volume transport is out of phase with that of Karimata Strait in the upper 300 m (Xu et al., 2021). The impact of seasonally varying monsoon winds on the Karimata Strait is evident from the vertical structure (Figure 8). Seasonally varying monsoonal rainfall and freshening strongly modulate the Karimata Strait. During summer (winter), the southward meridional flow at 1.05°S is weaker (stronger) and maximum value near the middle of strait within 2–40 m depth (entire column) (Figures 8a and 8b). The net flow is southwards for all the seasons and varies from 0.1 to 0.6 m/s. Temperature (Figures 8c and 8d), salinity (Figures 8e and 8f), and density (Figures 8g and 8h) structure show a pronounced summer-time two-layer structure separated around ~40 m depth. This two-layer structure is associated with the presence of a ~3°C temperature gradient and a 2 kg/m^3 density gradient vertically. This structure is related to the fact that MLD over the Karimata Strait is almost at a similar depth (Figures 2 and 8). The vertical gradient (i.e., two-layer structure) is diffused under the influence of strong transport and monsoon current. This is reflected in the vertical structure in the winter when the two-layer structure nearly vanishes in temperature, salinity, and density. Instead, a cooler water layer is seen east of 108°E and below 40 m depth. It is associated with high saline (and denser) water mass in the same region.

Lombok Strait is one of the outflows of the ITF that carries water from the Indonesian seas into the Indian Ocean (almost 30% of ITF) (Figures 2 and 9), contributing to the water delivering from the Pacific to the Indian Ocean (e.g., Potemra et al., 2003). Throughout the year, the water flows southward through Lombok Strait, however, the flow is stronger and deeper in winter relative to summer. The strength of the southward flow is maximum (~0.6 m/s) toward the western part of the strait and up to 100 m depth. This along strait velocity structure is consistent with the observations of Sprintall et al. (2009). The temperature (salinity) structure (Figure 9) shows a uniform warm (fresh) layer up to ~50 m depth that becomes deeper (~70 m) toward the eastern end. The density structure of the Lombok Strait follows the salinity structure, and displays no barrier layer formation.

All the above results demonstrate distinctive features of the different straits and indicate the possible role of stratification and vertical mixing. To unravel the seasonal stratification characteristics over the domain, we now examine the barrier layer formation (Figure S6).

The barrier layer hinders the turbulent entrainment of cold thermocline water into the surface mixed layer. Therefore, it serves to limit vertical mixing, allowing tropical air-sea interactions to progress with less impediment by SST cooling and boundary layer stabilization. The barrier layer is a climatological feature of the western equatorial Pacific (Cronin & McPhaden, 2002; Sprintall & Tomczak, 1992), however, it is only present in the SCS during strong mixing and shows a large spatial variability (Figure S2). Our results are consistent with Zeng and Wang (2017) and show that the different parts of the SCS and MC exhibit strong spatio-temporal variability in the barrier layer. The SCS barrier layer forms and maintains during summer and decays during winter (Zeng & Wang, 2017). The notable presence of the barrier layer is observed in the Luzon Strait, Makassar Strait, and east of Karimata Strait (Figure S7). Due to weaker wind in the northeastern basin than the rest of SCS, the Luzon Strait acts as a local flux regime (e.g., Alford et al., 2011). The barrier layer over the Luzon Strait is maintained by the intrusion of warm Kuroshio water associated with the accumulation of low-salinity water over the region. Unlike the Luzon Strait area, the Vietnam coast region is driven mostly by surface winds, and the barrier layer is controlled by freshwater and intense convergence. In winter, the barrier layer in the northern SCS is uniform due to moderate surface cooling, wind stirring, and the SCS western boundary current. The region around Mindoro Strait shows high barrier layer thickness in summer, which may be related to the combined impact of shallow MLD linked with intense downward Ekman pumping. It is consistent with Zeng & Wang (2017)'s inference on the role of local precipitation and Ekman pumping on the maintenance of the barrier layer in the eastern basin. Over the SCS, barrier layer thickness and upper ocean temperature have a linear correlation (Zeng & Wang, 2017).

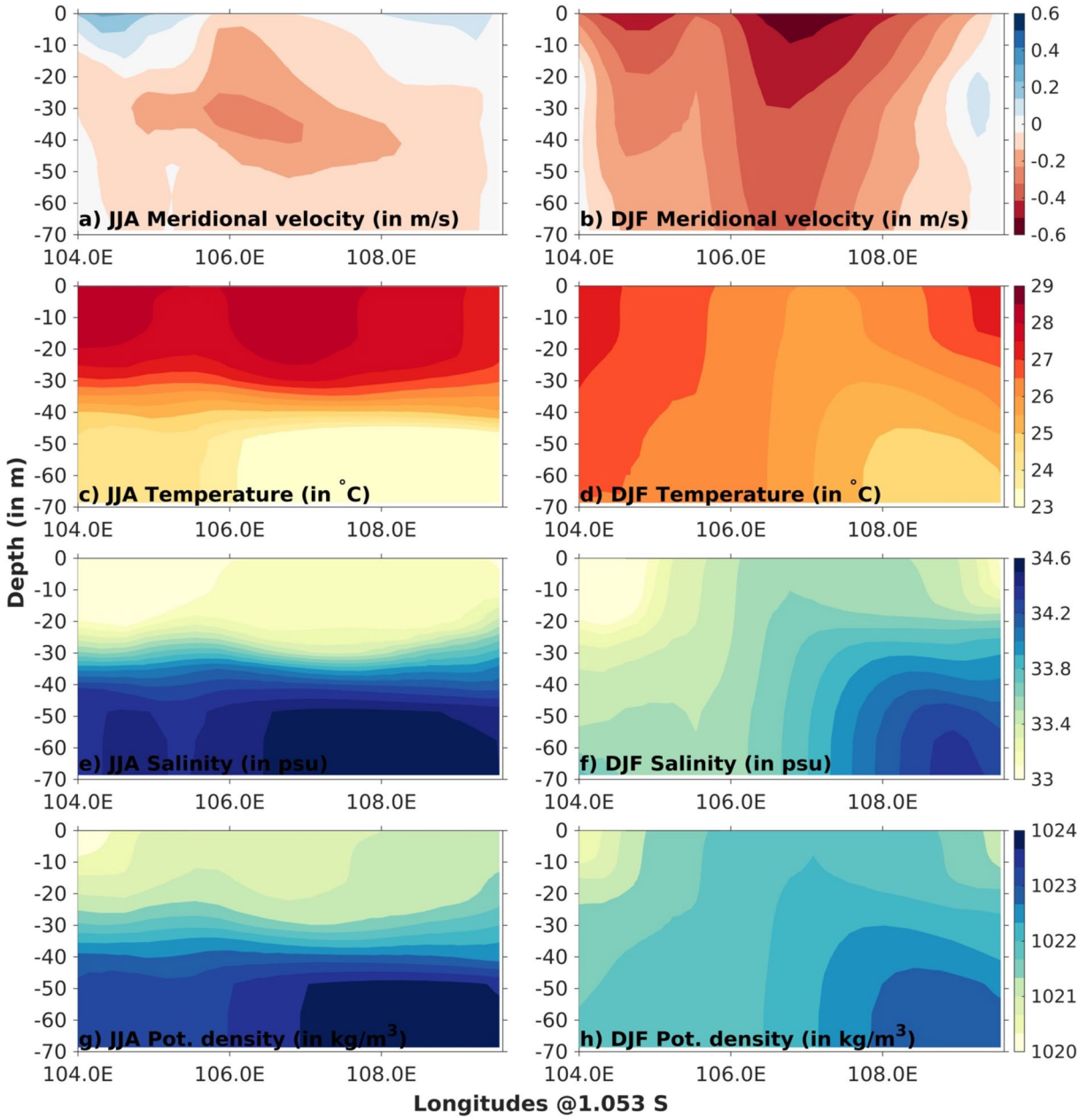

Figure 8. Seasonal climatological vertical structure of Karimata Strait at 1.053°S from regional ocean modelling system (ROMS) simulation. Climatology of (a and b) meridional velocity (in m/s), (c and d) temperature (in °C), (e and f) salinity (in psu), and (g and h) potential density (kg/m^3). Summer (JJA) and winter (DJF) seasons are shown in the left and right panel, respectively.

Overall, the presence of a barrier layer is closely related to surface wind stirring, freshwater, heating, and related oceanic processes.

Just how important is mixing over the domain, and what is its distribution along with that of the stratification? To answer that, we study the seasonal stratification as a function of Brunt-Väisälä frequency (in terms of N^2) in surface and subsurface layers. The knowledge of stratification in the upper waters of the SCS is sensitive to the MLD, isothermal layer depth, and barrier layer thickness (Zheng et al., 2016). The Brunt-Väisälä frequency values are vertically averaged for 0–50 m (Figures 10a and 10b) and 50–400 m (Figures 10c and 10d) for surface and subsurface stratifications, respectively. A higher Brunt-Väisälä frequency value suggests a higher degree of vertical stratification (i.e., more stable), which inhibits overturning.

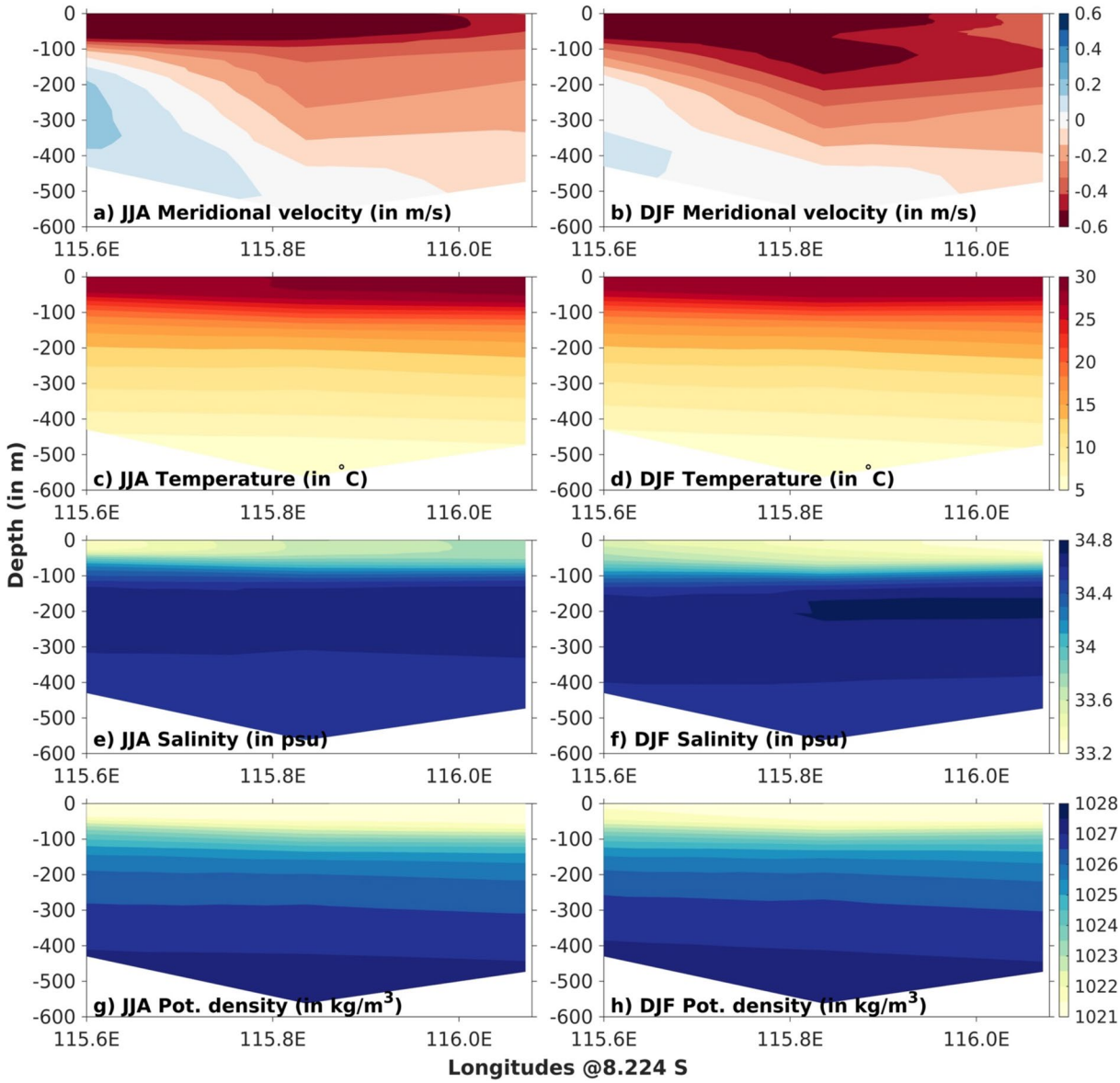

Figure 9. Seasonal climatological vertical structure of Lombok Strait at 8.224°S from regional ocean modelling system (ROMS) simulation. Climatology of (a and b) meridional velocity (in m/s), (c and d) temperature (in °C), (e and f) salinity (in psu), and (g and h) potential density (kg/m^3). Summer (JJA) and winter (DJF) seasons are shown in the left and right panel, respectively.

During the summer, almost the entire SCS region and Karimata Strait region show high stratification in the upper 50 m, which becomes near zero in the winter except near the Borneo coast. Historically some of the ocean's largest internal waves occur within the northern SCS. The higher N^2 values over Luzon Strait in the summer also indicate the presence of internal wave activity, which is consistent with earlier observational and modeling studies (e.g., DeCarlo et al., 2015). The subsurface layer (50–400 m) is almost uniform and shows a lower degree of stratification in both seasons, except the Vietnam upwelling region and Karimata Strait during the summer. These results also suggest the possible link between shallow regions with monsoon rainfall. As Karimata Strait connects to the ITF, this higher stratified water mass modulates the ITF water mass.

Because of the western Pacific Ocean's role in modulating the SCS water mass, it is now important to understand the characteristic of water mass near Luzon Strait. We study the water mass characteristics near the Luzon Strait in the next section.

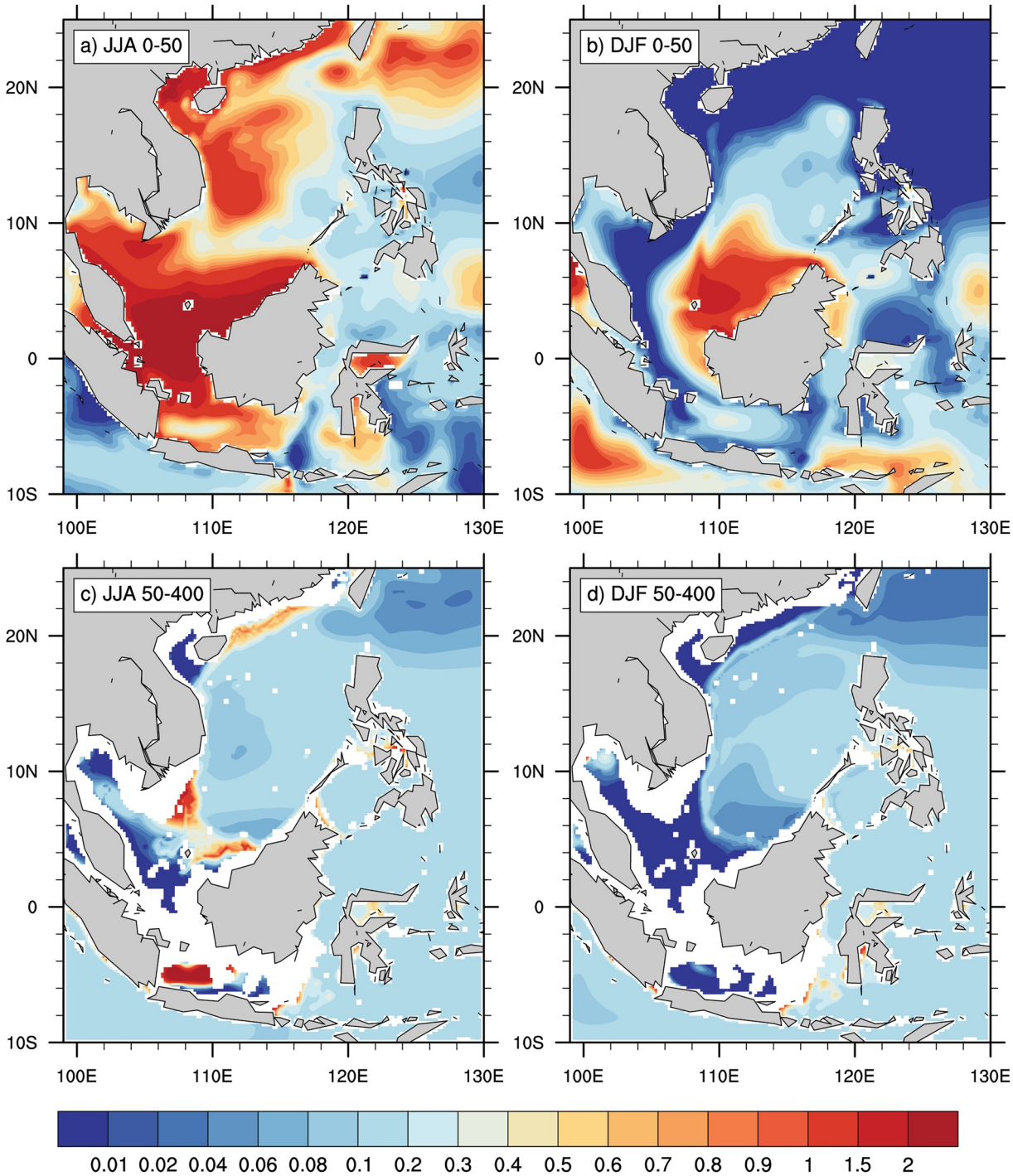

Figure 10. Seasonal climatological Brunt-Väisälä frequency (N^2 in 10^{-7} s^{-2}) from regional ocean modelling system (ROMS) simulation for (a and b) top 50 m averaged, and (c and d) 50–400 m averaged. a, c are for summer (JJA), and b, d is for winter (DJF). The regions shallower than 50 m are indicated by white color in c-d.

3.4. Identification of Cool Water Mass Across Luzon Strait

The T-S diagrams are used to identify the long-term mixing-free existence of deepwater masses at 20.5°N latitude across different longitudes of Luzon Strait (Figure 11). Other straits are not considered here as their depth is too shallow for deepwater exchange. Below 2000 m, direct water exchange between the SCS and Pacific through Luzon Strait is negligible (Figure 4). Therefore, deepwater in the SCS is affected by

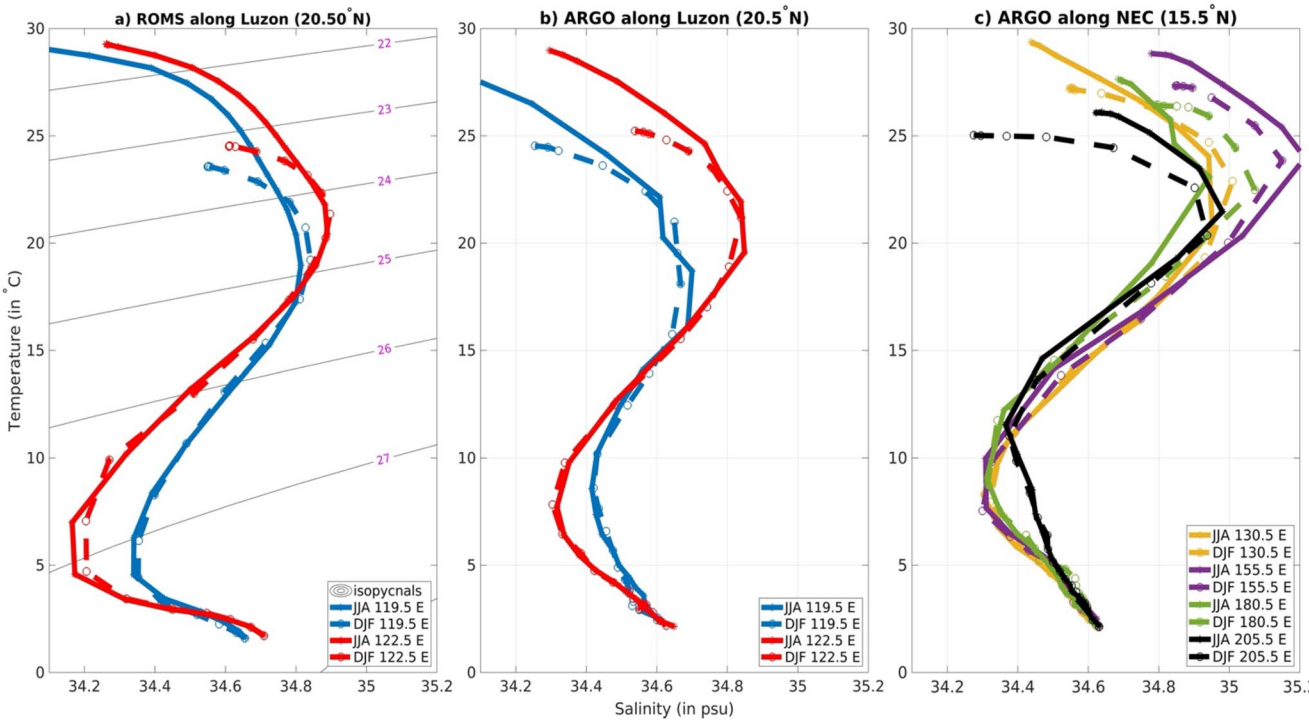

Figure 11. Seasonal climatological T-S diagram along Luzon Strait and NEC for summer (JJA; solid line) and winter (DJF; dotted line). T-S diagram from (a) regional ocean modelling system (ROMS) simulation at 20.5°N, (b) gridded Argo data at 20.5°N, and (c) gridded Argo data along NEC (15.5°N. Legends denote the season and longitudinal point. Black contours in (a) indicate isopycnals (in kg/m^3, based on $p = 0$). Leading "10" is always present in the density, therefore, not mentioned in general.

western Pacific upper-surface water (e.g., Chen et al., 2006; Deng et al., 2018). The modeled thermohaline structure indicates warm and low saline water in the surface layer (<50 m); warm and high saline water in the subsurface layer (~150–250 m); cool and low saline water in the intermediate layer (~400–1200 m); low temperature and high salinity in the deep layer (>1,500 m) (Figures 4 and 11a). During summer (JJA, Figures 11a), the near-surface temperature is maximum in the western Pacific at 20.5°N with a salinity of ~34.25 psu, and the temperature decreases as we move toward SCS. In the intermediate layer, this feature is more pronounced at different locations along 20.5°N. In the intermediate layer, the lowest salinity of 34.15 psu is observed for 122.5°E, whereas the lowest summer salinity is 34.3 psu for 119.5°E (i.e., denser than the western Pacific). The water mass characteristics between these two points are almost similar in the subsurface and deeper layers (Figures 11a). Both the seasons show a reversed "S" shaped T-S relationship in the ROMS simulations (Figures 11a), which is pretty consistent in the Argo observations (Figures 11b). The interpoint diversity along 20.5°N gets reduced with cooler winter surface temperature and the intermediate layer becomes more pronounced. Seasonal changes (from summer to winter) in the lowest salinity in the intermediate layer of SCS is about 0.09 psu. The highest saline water mass in the subsurface layer of SCS during winter becomes less dense (reduction of ~0.5 kg/m^3) relative to summer, even though the western Pacific shows no significant changes (Figures 11a and 11b). The salinity maximum water is characteristic of tropical north Pacific water (Suga et al., 2000), in the range of 24.5–25.5 kg/m^3 in summer and 24–25 kg/m^3 range in the winter. The salinity minimum zone is (~26–27 kg/m^3 density) is regarded as intermediate water that originates from North Pacific intermediate water (Wyrtki, 1961; You et al., 2005). The strong temperature and salinity gradients along the Luzon Strait have little role in modulating this high density-low saline water.

However, the presence of cool water mass in the deepwater of the SCS is not a surprising discovery as Luzon Strait is connected with the western Pacific Ocean and also reported in earlier studies (e.g., Chen et al., 2006; Deng et al., 2018; Nitani, 1972; Qu et al., 2000, 2004; 2006b). An earlier study showed that the deepwater west of Luzon Strait is completely flushed by intrusive non-SCS water from the lower layer of

Luzon Strait in 10–12 years (Liu & Gan, 2017). This water is hypothesized to induce upwelling in the far SCS basin to compensate for intrusive denser water in Luzon Strat (Fang et al., 2009). Qu et al., (2000) argued the Luzon Strait salinity minimum water (i.e., north Pacific intermediate water) enters during spring when north Pacific tropical water intrusion is weaker. Subduction of low-saline water mass in the SCS (e.g., Huang et al., 2018), and a recent water isotope based study (Wu et al., 2021) further provides a deeper understanding of the presence of Pacific water mass in the deep SCS layer.

Nonetheless, the seasonal climatological characteristics of deepwater mass along the Luzon Strait are not known in the literature, thereby, we provide an important insight here. Consequently, an important question arises: how far can we track this SCS deepwater mass? To address that we studied the T-S relationship beyond the ROMS domain boundary and along the NEC region from Argo observations (Figures 11c). We found the intriguing presence of similarly deep and cool water mass up to 180°E over the NEC region, beyond which this water mass characteristic is missing. To further verify the source and pathway of the deepwater mass we examined the T-S diagram in different locations north and south of NEC. However, moving northward or southward of NEC shows a different nature of deepwater mass (Figure S8). It demonstrates the origin of SCS deepwater mass lies in the far eastern region of the central Pacific Ocean, and NEC acts as the carrier of that water mass (see the schematic in Figure S8d).

Now using ROMS simulations we have a better understanding of transports across different straits of the SCS and MC, and their associated dynamics. We also unravel the seasonality and origin of deepwater mass in the SCS at the present. But we do not know whether or not these oceanic characteristics of the region will be the same in the future. Therefore, it is critical to understand how anthropogenic forcing can module the regional ocean transports and upper ocean behavior.

3.5. Future Changes in Ocean Transports and Upper Ocean Behavior

First, we noted the reasonable match of seasonal zonal and meridional volume transport in each HighResMIP model while compared to ROMS and earlier studies (see Figure S9 and Section 3.2). Next, using a multimodel ensemble, we quantify the seasonal climatological changes by the end of the 21st century as the difference between the end-of-the-century and present (i.e., 2071–2100 minus 1981–2010). We focus on the horizontal mass and heat transport over the region. A significant amount of mass and heat transport from the western Pacific Ocean to the SCS through the Luzon Strait, subsequently impacts the ITF (Tozuka et al., 2007) and modulates a coupled climate system over the region (Sprintall et al., 2019). The climatological surface mass transport (Figures S10a–S10b) resembles the surface current patterns. The mass transport changes (Figure 12a) show a stronger northward transport along the Vietnam coast and a significant increase in southward transport along the western boundary of the SCS during the winter (Figures 12b and S11). It may be linked to the intensification of the western boundary currents due to climate change-induced expansion of the Hadley cell (e.g., Seager & Simpson, 2016). Heat transport (Figures 12c–12d, and S12) shows a notable increase in Luzon transport and reduction in Makassar Strait relative to the climatology (Figure S10c–S10d). These changes in heat transport are stronger in the winter and associated with wintertime southward flow along the western boundary (i.e., along the Vietnam coast), where we noted an increase in mass transport. Heat convergence and associate increase over the Vietnam coast (~13°N) during summer are also notable. As SCS plays as a conveyor of heat and freshwater transport, these changes will likely impact the ITF throughflow and transport to the Indian Ocean.

As the changes in heat transport patterns are not uniform throughout the region, it is expected that different straits in the region will experience various degrees of change. We now explore the seasonal time evolution of such changes in heat transport from 1850 to 2100 (Figure 13). It is clear that despite the presence of multi-decadal variability, heat transport will have a large change by the end of the century for most of the straits. These time series are smoothed by 20-years (Figure 13 *X*-axis is for 1860–2090), therefore, the effect of high-frequency variability (e.g., Sprintall et al., 2019) is excluded. The heat transport changes across these straits are summarized in Table 1. Overall, meridional winter time changes are more pronounced than in summer. Our results indicate a substantial increase in heat transport through the Luzon Strait (up to ~40%), wintertime Karimata Strait (~11%), and wintertime southward Mindoro Strait (up to ~400%). Whereas in winter, a substantial decrease in heat transport through Makassar (up to ~55%) and Lombok (up to ~75%)

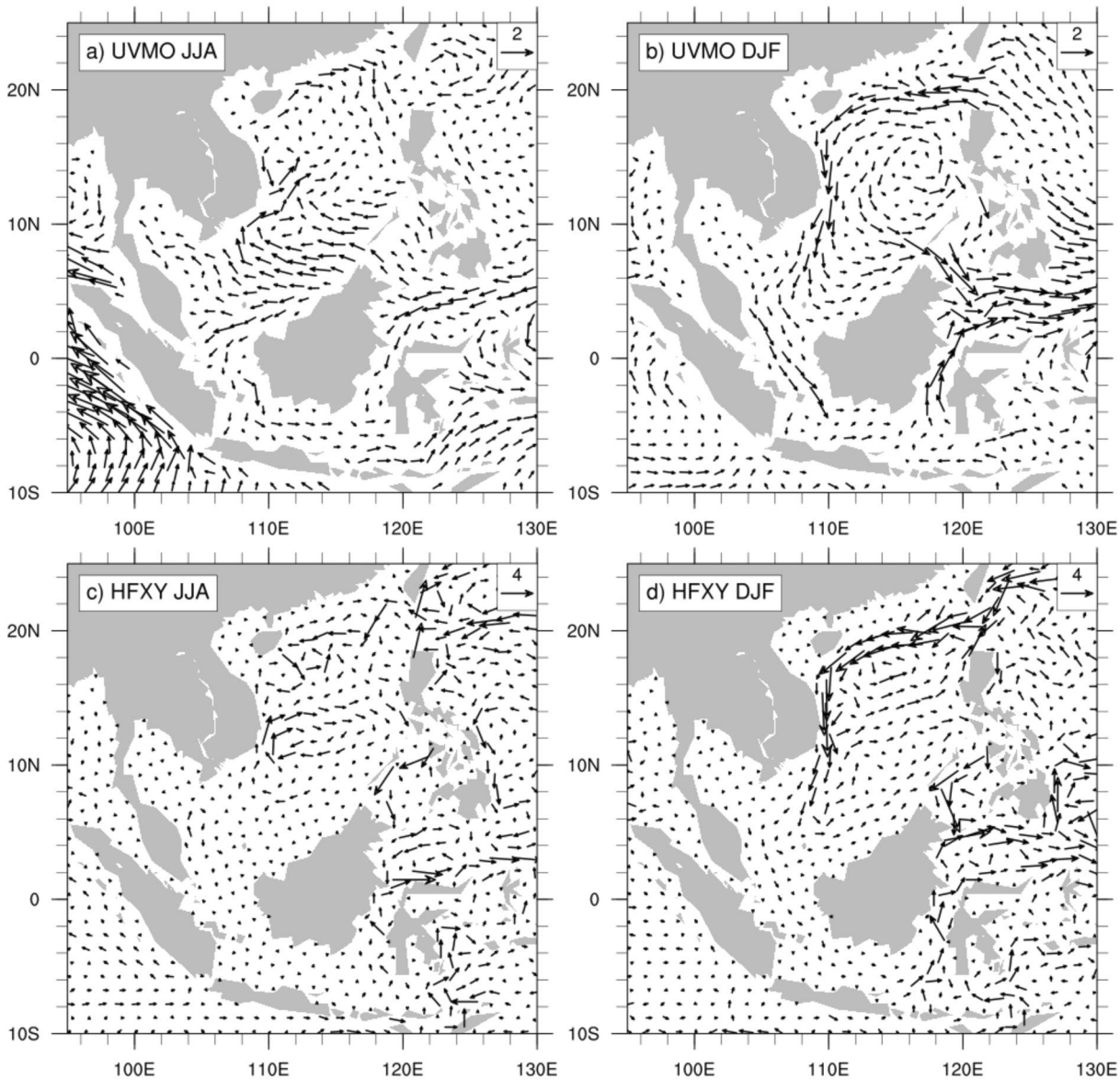

Figure 12. Seasonal climatological changes (2071–2100 minus 1981–2010) in (a and b) surface mass transport (in kg/s), and (c and d) heat transport (in 10^{13} W) from the multimodel ensemble of HighResMIP models. Projection data is for the SSP5-585 scenario. Summer (JJA) is displayed in a, c, and winter (DJF) in b,d.

Straits. The magnitude of all these projected changes (Table 1) are relative to the 1981–2010 period and may change for a different reference period.

Here the location of Karimata Strait transport is different from the cross-section plot (Figure 8), as we aim to see transport changes in the Java sea, just before meeting the Makassar Strait branch of the ITF. Interestingly, El Niño-Southern Oscillation (ENSO) and Indian Ocean Dipole (IOD) have an insignificant correlation with interannual variability of the Karimata Strait transport (Xu et al., 2021). However, Xu et al. (2021) found a decrease in volume and heat transport during 1997–2015. We find a similar summertime reduction in zonal heat transport change (Figure 13a). It is noteworthy that the southward heat transport through the ITF (mainly through Makassar Strait) in winter is smaller than summer and its annual value (Figure S10; Xu et al., 2021), implying significant wintertime contribution from Karimata Strait. As heat transport in the Makassar Strait in winter is projected to weaken drastically, our results (see Table 1 and Figure 13) suggest the important role of the Karimata Strait in the coming decades and a potential increase in heat transport to the Java Sea during winter.

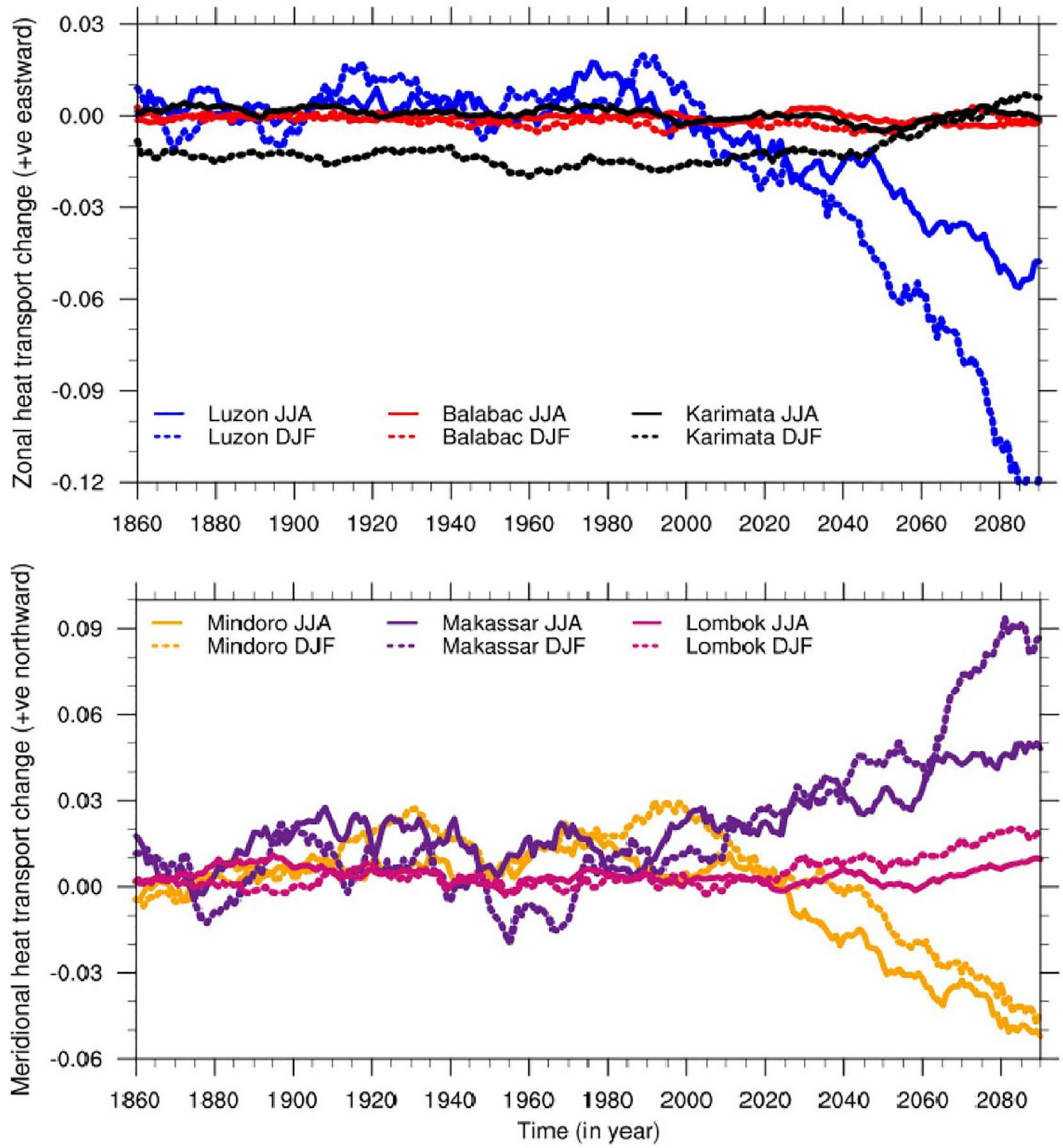

Figure 13. Time series of heat transport change (in PW; relative to 1859) for (a) zonal and (b) meridional component from the multimodel ensemble of HighResMIP across different straits. Luzon (18–22°N, 120–121°E), Mindoro (11–13°N, 119–122°E), Balabac (6.5–8.5°N, 117–118°E), Makassar Strait (2 °S-1 °S, 116–119.5 °E), Karimata Strait (7 °S-3°S, 111–112°E), Lombok Strait (9°S–8°S, 115°E–116.5°E). The 1850–2100 time series are smoothed by 20 years of running average before calculating relative change. Projection data is for the SSP5-585 scenario.

Due to the convergence of heat transport in the SCS, it is expected that the upper ocean heat content of the domain will increase by the end of the century. The increase in heat content is also likely to be non-uniform as heat transport changes are not uniform over the domain. Indeed this is evident in the upper ocean heat content change (Figures 14a and 14b). Our results show up to a 3.5 GJ/m^2 increase in heat content relative to the climatology (Figure S13a–S13b). Essentially the earlier studies also argued that the upper ocean heat content increase is the result of ocean circulation and transport changes, where the role of vertical mixing is secondary (e.g., Dias et al., 2020). We also note greater warming in the summer than in winter (Figures 14a and 14b). Further, as more volume can contain greater heat, the regions of higher heat content increase are also deeper (Figures 1, 14a–14b). SSS changes relative to climatology (Figures 14c–14d, S13c–S13d) suggest freshening of the surface layer of the ocean by the 21st century (Figures 14c and 14d) for both summer and winter with a dominance in the western Pacific region. It may be attributed to the intrusion of more fresh-water from the western Pacific Ocean to SCS and the western part of ITF as evident in Figure 12. It may

Table 1
Summary of Average Seasonal Heat Transport Change in % ([2071–2010 Minus 1981–2010]/[2071–2010]) Across Different Straits From HighResMIP Multimodel Ensemble Under the SSP5-585 Scenario

Strait	Component of heat transport	Climatological direction of heat transport in the present (1981–2010) in summer (winter)	% Change relative to present	
			Summer	Winter
Luzon	Zonal	West (West)	+37.99%	+33.07%
Balabac		East (West)	**−20.29%**	**−9.90%**
Karimata		West (East)	**−0.11%**	11.86%
Mindoro	Meridional	North (North)	**−85.36%**	**−410.54%**
Makassar		South (South)	**−5.76%**	**−55.51%**
Lombok		South (South)	**−2.08%**	**−74.10%**

Note. The changes are calculated over the box mentioned in Figure 13 caption from the zonal and meridional heat transport time series without smoothing. The "+ve" ("-ve") sign in % change suggests the end-of-the-century value in the same (opposite) direction as in the present. Negative % changes (i.e., reductions) are indicated in bold.

be also associated with a higher amount of oceanic rainfall due to higher SST and upper ocean heat content. In addition to the increased ocean temperature, salinity changes contribute to the stratification locally (Li, Cheng et al., 2020). Interestingly, SCS was one of the most significant freshening regions during the 1950–2000 period (Durack et al., 2012), with a possible role of weakening Kuroshio intrusion over the northern region (e.g., Nan et al., 2013). Here we argue that the SCS and MC will experience increased stratifications in the region by the end of the 21st century, consistent with the increased global stratification over the past half-century (e.g., Fu et al., 2016; Li, Cheng et al., 2020), and CMIP5 based projections (e.g., Moore et al., 2018). Further, MLD changes (Figures 14e and 14f) suggest a reduction in vertical mixing over the entire domain. Whereas, the strength of the increased near-surface density stratification can be a key contributor to the shallower MLD over the region by the end of the 21st century. Previously, DeCarlo et al. (2015) pointed out that the warming of the upper ∼100 m of the ocean can modulate changes in internal wave activity in the northern SCS. Projected MLD also shows a notable presence of a north-south gradient in both the seasons (Figures 14e and 14f). During summer (winter) MLD over the MC (northern SCS) is deeper than the northern SCS (MC) by ∼8 m. It may be related to the strengthening of monsoon wind over the region.

Projected upper ocean changes as shown here (Figures 13 and 14, and S14 and S15) have several critical implications. As the ocean and atmosphere are coupled systems, we cannot deny the role of atmospheric forcing (e.g., Liu et al., 2014; Xie et al., 2003) on these projected regional oceanic changes. Nonetheless, our results demonstrate clear evidence of how oceanic transports and upper ocean dynamics over the region may change by the end of the 21st century. Further, due to the critical role of the Indonesian Archipelago as both a maritime "chokepoint" of global ocean circulation and as a critical driver of the regional water cycle (Lee et al., 2019), the potential air-sea interaction modifications could have significant impacts over the region and beyond.

4. Summary and Future Outlook

Using a climatological ROMS simulation, seasonal transports across the six straits of the SCS and MC are studied in terms of their regional drivers. We examined the vertical structure of these straits in summer and winter. The structure and transports across these straits are largely determined by bathymetry (from ∼70 m in Karimata to ∼2,500 m in Luzon Strait), monsoonal winds, and strong stratifications. We found the intermediate and deep layers of water mass of the Luzon Strait can be tracked up to the source region in the central Pacific Ocean. Further, we investigate projected changes in mass and heat transport, and upper ocean behavior at the end of the 21st century using the HighResMIP simulation under the SSP5-585 scenario. We revealed a pronounced increase (decrease) in heat transport through Luzon and wintertime Karimata Strait (Makassar and Lombok Strait) in the future projection. These transport changes are also associated with pronounced modulation in the regional upper ocean characteristics, such as shallower MLD and fresher SSS.

In this study, we only focus on climatological features and long-term projected changes. However, we recognize that the SCS and MC are also modulated by tropical climate variabilities in different timescales, such as ENSO (Gordon et al., 2012; Jiang et al., 2019; Qu et al., 2004; Ramos et al., 2019), IOD (e.g., Li, Gordon et al., 2020), Pacific Decadal Oscillation (Wu, 2013), Interdecadal Pacific Oscillation (e.g., Li, Gordon et al., 2020), and Philippines-Taiwan oscillation (Chang & Oey, 2012). Furthermore, due to the potential role of oceanic mesoscale eddies (Zhang et al., 2016), SCS transport may also change in the future. It remains unanswered how these climate and ocean drivers will impact the SCS and MC transports by the end of the 21st century.

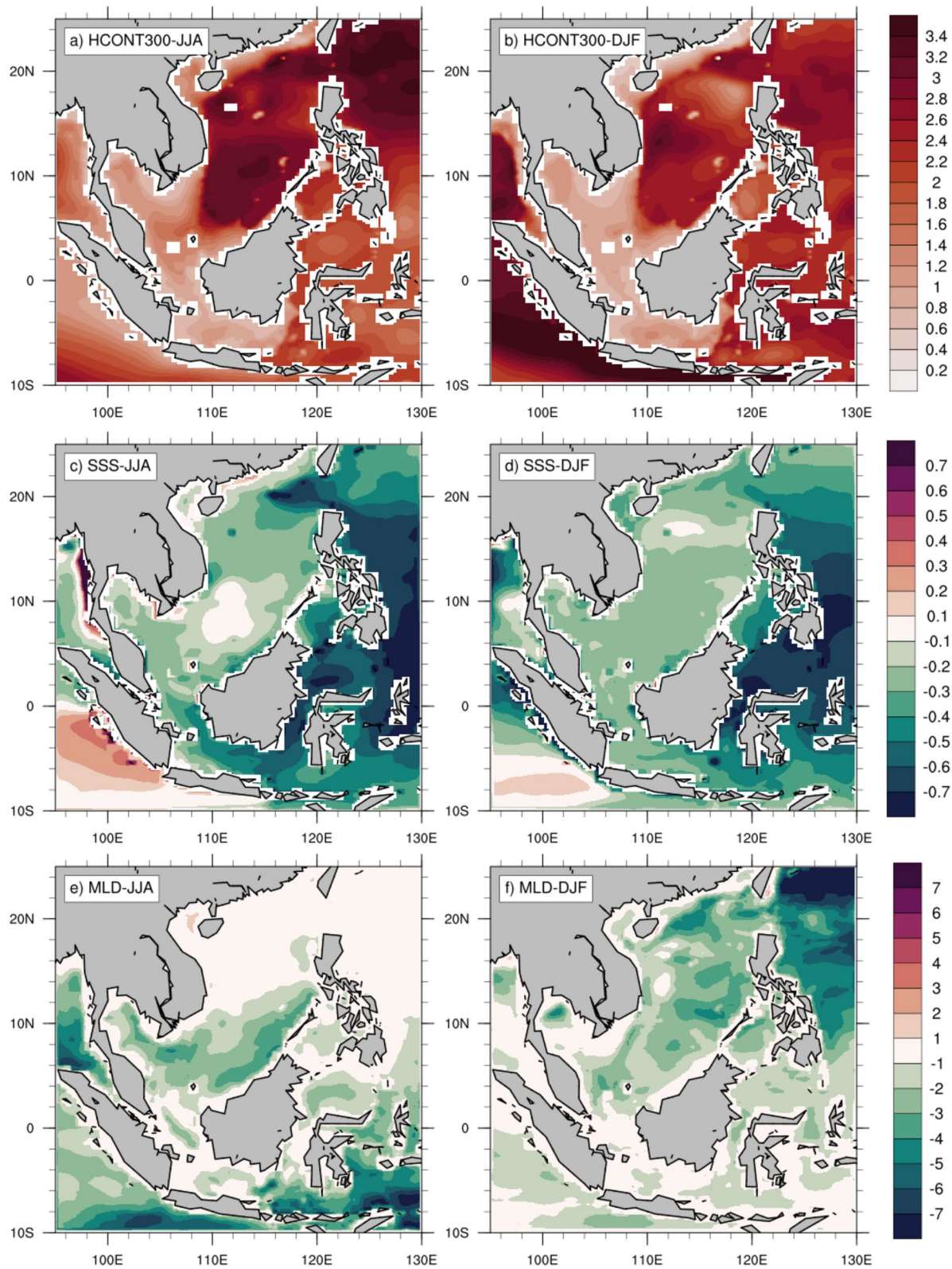

Figure 14. Seasonal climatological changes (2071–2100 minus 1981–2010) in upper ocean behavior at the end of the 21st century from HighResMIP multimodel ensemble. Changes in (a–b) top 300 m averaged heat content (HCONT300; in 10^9 J/m^2), (c–d) sea surface salinity (SSS; in psu), and (e–f) mixed layer depth (MLD; in m. Projection data is for the SSP5-585 scenario. The MLD in these HighResMIP models is defined by potential density criteria referenced to the ocean surface. Summer (JJA) and winter (DJF) seasons are shown in the left and right panel, respectively.

The global thermohaline circulation is known to contribute ~5.7 Sv to the ITF due to wind-driven upwelling in the Indo-Pacific Antarctic Circumpolar Current region (Shriver & Hurlburt, 1997). Therefore, it would be also interesting to explore how this interaction is going to modulate if global thermohaline circulation weakens due to climate change. The transports across SCS and ITF are critical not only for regional climate variability, but also for the broader Indo-Pacific region, and beyond. As continued anthropogenic warming is likely to increase the upper ocean heat content further (Figure 14), there are potentially serious consequences for biogeochemical changes and sea-level rise, particularly over the SCS and MC. We believe our results on projected changes to transport and ocean behavior will be instrumental in triggering more research over Southeast Asia. On the other hand, increasing horizontal resolution in regional ocean models can improve the upper ocean behavior, but it may fail to reasonably capture the interannual to decadal variabilities (e.g., Jiang et al., 2019). Therefore, careful design of further regional model simulation studies is needed to represent multiscale processes with complex terrain over the SCS and MC.

Data Availability Statement

ETOPO1 1 Arc minute global relief model data (1/60°; Amante & Eakins, 2009) data is available from https://www.ngdc.noaa.gov/mgg/global/. NOAA OI SST v2 data is available from https://psl.noaa.gov/data/gridded/data.noaa.oisst.v2.highres.html. SODA v3.3.1 reanalysis is available from http://apdrc.soest.hawaii.edu/datadoc/soda_3.3.1.php. SCSPOD14 data is available from https://figshare.com/collections/Data_for_SCSPOD14_a_South_China_Sea_physical_oceanographic_dataset_derived_from_in_situ_measurements_during_1919_2014/1513842. WOD data is available from NOAA site https://www.ncei.noaa.gov/products/world-ocean-database. Gridded Argo products (MOAA GPV) are available from JAMESTEC site http://www.godac.jamstec.go.jp/argogpv/e/. OA flux products are available from http://apdrc.soest.hawaii.edu/datadoc/whoi_oafluxmon.php. CMIP6 HighResMIP model data is available from https://esgf-node.llnl.gov/search/cmip6/. ROMS simulation data is available from https://figshare.com/s/667f4a2e0679198a8d3b.

Acknowledgments
This is Earth Observatory of Singapore contribution number 398. This research was funded by the Singapore Ministry of Education (MOE) Academic Research Fund Tier 2 Project MOE2016-T2-1-016 and Earth Observatory of Singapore. It was also partially supported by MOE Tier 3 Project MOE2019-T3-1-004 funded at Earth Observatory of Singapore. The authors acknowledge the World Climate Research Programme, which, through its Working Group on Coupled Modelling, coordinated and promoted CMIP6. The authors thank the climate modelling groups for producing and making available their model output, the Earth System Grid Federation (ESGF) for archiving the data and providing access, and the multiple funding agencies that support CMIP6 and ESGF. Figures were created using Matlab 2020a and NCAR Command Language (version 6.6.2) [Software] (2019). Boulder, Colorado: UCAR/NCAR/CISL/TDD. https://doi.org/10.5065/D6WD3XH5

References

Alford, M. H., MacKinnon, J. A., Nash, J. D., Simmons, H., Pickering, A., Klymak, J. M., et al. (2011). Energy flux and dissipation in Luzon Strait: Two tales of two ridges. *Journal of Physical Oceanography*, *41*(11), 2211–2222. https://doi.org/10.1175/jpo-d-11-073.1

Amante, C., & Eakins, B. W. (2009). ETOPO1 1 arc-minute global relief model: Procedures, data sources and analysis. *NOAA technical memorandum NESDIS NGDC-24*. National geophysical data center. https://doi.org/10.7289/V5C8276M

Blanke, B., Roy, C., Penven, P., Speich, S., McWilliams, J., & Nelson, G. (2002). Linking wind and interannual upwelling variability in a regional model of the southern Benguela. *Geophysical Research Letters*, *29*(24), 41–1. https://doi.org/10.1029/2002gl015718

Chang, Y. L., & Oey, L. Y. (2012). The Philippines–Taiwan Oscillation: Monsoonlike interannual oscillation of the subtropical–tropical western North Pacific wind system and its impact on the ocean. *Journal of Climate*, *25*(5), 1597–1618. https://doi.org/10.1175/jcli-d-11-00158.1

Chen, C. T. A., Wang, S. L., Chou, W. C., & Sheu, D. D. (2006). Carbonate chemistry and projected future changes in pH and $CaCO_3$ saturation state of the South China Sea. *Marine Chemistry*, *101*(3–4), 277–305. https://doi.org/10.1016/j.marchem.2006.01.007

Chu, P. C., Edmons, N. L., & Fan, C. (1999). Dynamical mechanisms for the South China Sea seasonal circulation and thermohaline variabilities. *Journal of Physical Oceanography*, *29*(11), 2971–2989. https://doi.org/10.1175/1520-0485(1999)029<2971:dmftsc>2.0.co;2

Chu, P. C., & Li, R. F. (2000). South China Sea isopycnal-surface circulation. *Journal of Physical Oceanography*, *30*(9), 2419–2438. https://doi.org/10.1175/1520-0485(2000)030<2419:scsisc>2.0.co;2

Cronin, M. F., & McPhaden, M. J. (2002). Barrier layer formation during westerly wind bursts. *Journal of Geophysical Research*, *107*(C12). https://doi.org/10.1029/2001jc001171

Da Silva, A. M., Young, C. C., & Levitus, S. (1994). *Algorithms and Procedures* (Vol. 16, pp. 20910–23282). Atlas of surface marine data 1994.

De Boyer Montégut, C., Madec, G., Fischer, A. S., Lazar, A., & Iudicone, D. (2004). Mixed layer depth over the global ocean: An examination of profile data and a profile–based climatology. *Journal of Geophysical Research*, *109*, C12003. https://doi.org/10.1029/2004JC002378

DeCarlo, T. M., Karnauskas, K. B., Davis, K. A., & Wong, G. T. (2015). Climate modulates internal wave activity in the Northern South China Sea. *Geophysical Research Letters*, *42*(3), 831–838. https://doi.org/10.1002/2014gl062522

Deng, H., Huang, P., Tanhua, T., Stöven, T., Ke, H., Guo, W., et al. (2018). Observations of the intermediate water exchange between the South China Sea and the Pacific Ocean deduced from transient tracer measurements. *Journal of Geophysical Research: Oceans*, *123*(10), 7495–7510. https://doi.org/10.1029/2018jc014103

Dey, S. P., Dash, M. K., Sasmal, K., Jana, S., & Raju, N. J. (2020). Impact of river runoff on seasonal sea level, Kelvin waves, and East India Coastal Current in the Bay of Bengal: A numerical study using ROMS. *Regional Studies in Marine Science*, 101214. https://doi.org/10.1016/j.rsma.2020.101214

Dias, F. B., Fiedler, R., Marsland, S. J., Domingues, C. M., Clément, L., Rintoul, S. R., et al. (2020). Ocean heat storage in response to changing ocean circulation processes. *Journal of Climate*, *33*(21), 9065–9082. https://doi.org/10.1175/jcli-d-19-1016.1

Ding, X., Bassinot, F., Guichard, F., & Fang, N. Q. (2013). Indonesian throughflow and monsoon activity records in the Timor Sea since the last glacial maximum. *Marine Micropaleontology*, *101*, 115–126. https://doi.org/10.1016/j.marmicro.2013.02.003

Durack, P. J., Wijffels, S. E., & Matear, R. J. (2012). Ocean salinities reveal strong global water cycle intensification during 1950 to 2000. *Science*, *336*(6080), 455–458. https://doi.org/10.1126/science.1212222

Eyring, V., Bony, S., Meehl, G. A., Senior, C. A., Stevens, B., Stouffer, R. J., & Taylor, K. E. (2016). Overview of the Coupled Model Intercomparison Project Phase 6 (CMIP6) experimental design and organization. *Geoscientific Model Development*, *9*(5), 1937–1958. https://doi.org/10.5194/gmd-9-1937-2016

Fan, W., Jian, Z., Bassinot, F., & Chu, Z. (2013). Holocene centennial-scale changes of the Indonesian and South China Sea through flows: Evidences from the Makassar Strait. *Global and Planetary Change*, *111*, 111–117. https://doi.org/10.1016/j.gloplacha.2013.08.017

Fan, W., Song, J., & Li, S. (2014). A numerical study on seasonal variations of the thermocline in the South China Sea based on the ROMS. *Acta Oceanologica Sinica*, *33*(7), 56–64. https://doi.org/10.1007/s13131-014-0504-8

Fang, G., Susanto, D., Soesilo, I., Zheng, Q. A., Fangli, Q., & Zexun, W. (2005). A note on the South China Sea shallow interocean circulation. *Advances in Atmospheric Sciences*, *22*(6), 946–954.

Fang, G., Susanto, R. D., Wirasantosa, S., Qiao, F., Supangat, A., Fan, B., & Li, S. (2010). Volume, heat, and freshwater transports from the South China Sea to Indonesian seas in the boreal winter of 2007–2008. *Journal of Geophysical Research*, *115*(C12). https://doi.org/10.1029/2010jc006225

Fang, G., Wang, Y., Wei, Z., Fang, Y., Qiao, F., & Hu, X. (2009). Interocean circulation and heat and freshwater budgets of the South China Sea based on a numerical model. *Dynamics of Atmospheres and Oceans*, *47*(1–3), 55–72. https://doi.org/10.1016/j.dynatmoce.2008.09.003

Fasullo, J. T., Gent, P. R., & Nerem, R. S. (2020). Forced patterns of sea level rise in the community earth system model large ensemble from 1920 to 2100. *Journal of Geophysical Research: Oceans*, *125*(6), e2019JC016030. https://doi.org/10.1029/2019jc016030

Ferrol-Schulte, D., Gorris, P., Baitoningsih, W., Adhuri, D. S., & Ferse, S. C. (2015). Coastal livelihood vulnerability to marine resource degradation: A review of the Indonesian national coastal and marine policy framework. *Marine Policy*, *52*, 163–171. https://doi.org/10.1016/j.marpol.2014.09.026

Ffield, A., Vranes, K., Gordon, A. L., Dwi Susanto, R., & Garzoli, S. L. (2000). Temperature variability within Makassar Strait. *Geophysical Research Letters*, *27*(2), 237–240. https://doi.org/10.1029/1999gl002377

Fu, W., Randerson, J. T., & Moore, J. K. (2016). Climate change impacts on net primary production (NPP) and export production (EP) regulated by increasing stratification and phytoplankton community structure in the CMIP5 models. *Biogeosciences*, *13*(18), 5151–5170. https://doi.org/10.5194/bg-13-5151-2016

Gamage, R. N. (2016). Blue economy in Southeast Asia: Oceans as the new Frontier of economic development. *Maritime Affairs: Journal of the National Maritime Foundation of India*, *12*(2), 1–15. https://doi.org/10.1080/09733159.2016.1244361

Gan, J., Liu, Z., & Hui, C. R. (2016). A three-layer alternating spinning circulation in the South China Sea. *Journal of Physical Oceanography*, *46*(8), 2309–2315. https://doi.org/10.1175/jpo-d-16-0044.1

Gordon, A. L. (2005). The Indonesian Seas. *Oceanography*, *18*(4), 14–27. https://doi.org/10.5670/oceanog.2005.01

Gordon, A. L., Huber, B. A., Metzger, E. J., Susanto, R. D., Hurlburt, H. E., & Adi, T. R. (2012). South China Sea through flow impact on the Indonesian through flow. *Geophysical Research Letters*, *39*(11). https://doi.org/10.1029/2012gl052021

Gordon, A. L., Napitu, A., Huber, B. A., Gruenburg, L. K., Pujiana, K., Agustiadi, T., et al. (2019). Makassar Strait throughflow seasonal and interannual variability: An overview. *Journal of Geophysical Research: Oceans*, *124*(6), 3724–3736. https://doi.org/10.1029/2018jc014502

Gordon, A. L., Sprintall, J., & Ffield, A. (2011). Regional oceanography of the Philippine Archipelago. *Oceanography*, *24*(1), 14–27. https://doi.org/10.5670/oceanog.2011.01

Gordon, A. L., Sprintall, J., Van Aken, H. M., Susanto, D., Wijffels, S., Molcard, R., et al. (2010). The Indonesian throughflow during 2004–2006 as observed by the INSTANT program. *Dynamics of Atmospheres and Oceans*, *50*(2), 115–128. https://doi.org/10.1016/j.dynatmoce.2009.12.002

Gordon, A. L., & Susanto, R. D. (1998). Makassar Strait transport: Initial estimate based on Arlindo results. *Marine Technology SocietyMarine Technology Society Journal*, *32*(4), 34.

Gordon, A. L., Susanto, R. D., & Ffield, A. (1999). Throughflow within Makassar Strait. *Geophysical Research Letters*, *26*(21), 3325–3328. https://doi.org/10.1029/1999gl002340

Gordon, A. L., Susanto, R. D., Ffield, A., Huber, B. A., Pranowo, W., & Wirasantosa, S., (2008). Makassar Strait throughflow, 2004 to 2006. *Geophysical Research Letters*, *35*(24).

Guo, Z. X., & Fang, W. D. (1988). The transport of Kuroshio in the Luzon Strait in September 1985. *Tropic Oceanography*, *7*(2), 13–19.

Gutjahr, O., Putrasahan, D., Lohmann, K., Jungclaus, J. H., von Storch, J. S., Brüggemann, N., & Stössel, A. (2019). Max Planck Institute Earth System Model (MPI-ESM1. 2) for High-Resolution Model Intercomparison Project (HighResMIP). *Geophysical Model Development*, *12*, 3241–3281. https://doi.org/10.5194/gmd-12-3241-2019

Haarsma, R. J., Roberts, M. J., Vidale, P. L., Senior, C. A., Bellucci, A., Bao, Q., et al. (2016). High resolution model intercomparison project (HighResMIP v1. 0) for CMIP6. *Geoscientific Model Development*, *9*(11), 4185–4208. https://doi.org/10.5194/gmd-9-4185-2016

Haidvogel, D. B., Arango, H. G., Hedstrom, K., Beckmann, A., Malanotte-Rizzoli, P., & Shchepetkin, A. F. (2000). Model evaluation experiments in the North Atlantic Basin: Simulations in nonlinear terrain-following coordinates. *Dynamics of Atmospheres and Oceans*, *32*(3–4), 239–281. https://doi.org/10.1016/s0377-0265(00)00049-x

Hosoda, S., Ohira, T., & Nakamura, T. (2008). A monthly mean dataset of global oceanic temperature and salinity derived from Argo float observations. *JAMSTEC Report of Research and Development*, *8*, 47–59. https://doi.org/10.5918/jamstecr.8.47

Hsin, Y. C., Wu, C. R., & Chao, S. Y. (2012). An updated examination of the Luzon Strait transport. *Journal of Geophysical Research: Oceans*, *117*(C3). https://doi.org/10.1029/2011jc007714

Huang, Z., Zhuang, W., Liu, H., & Hu, J. (2018). Subduction of a low-salinity water mass around the Xisha Islands in the South China Sea. *Scientific Reports*, *8*(1), 1–9. https://doi.org/10.1038/s41598-018-21364-3

Jackett, D. R., McDougall, T. J., Feistel, R., Wright, D. G., & Griffies, S. M. (2006). Algorithms for density, potential temperature, conservative temperature, and the freezing temperature of seawater. *Journal of Atmospheric and Oceanic Technology*, *23*(12), 1709–1728. https://doi.org/10.1175/jtech1946.1

Jian, L., Xianwen, B., & Guoping, G. (2004). Optimal estimation of zonal velocity and transport through Luzon Strait using variational data assimilation technique. *Chinese Journal of Oceanology and Limnology*, *22*(4), 335–339. https://doi.org/10.1007/bf02843626

Jiang, G. Q., Wei, J., Malanotte-Rizzoli, P., Li, M., & Gordon, A. L. (2019). Seasonal and interannual variability of the subsurface velocity profile of the Indonesian Throughflow at Makassar Strait. *Journal of Geophysical Research: Oceans*, *124*(12), 9644–9657. https://doi.org/10.1029/2018jc014884

Jiang, Y., Zhang, S., Tian, J., Zhang, Z., Gan, J., & Wu, C. R. (2020). An examination of circulation characteristics in the Luzon Strait and the South China Sea using high-resolution regional atmosphere-ocean coupled models. *Journal of Geophysical Research: Oceans*, *125*(6), e2020JC016253. https://doi.org/10.1029/2020jc016253

Jilan, S. (2004). Overview of the South China Sea circulation and its influence on the coastal physical oceanography outside the Pearl River Estuary. *Continental Shelf Research*, *24*(16), 1745–1760. https://doi.org/10.1016/j.csr.2004.06.005

Kwiatkowski, L., Torres, O., Bopp, L., Aumont, O., Chamberlain, M., Christian, J. R., et al. (2020). Twenty-first century ocean warming, acidification, deoxygenation, and upper-ocean nutrient and primary production decline from CMIP6 model projections. *Biogeosciences*, *17*(13), 3439–3470. https://doi.org/10.5194/bg-17-3439-2020

Large, W. G., McWilliams, J. C., & Doney, S. C. (1994). Oceanic vertical mixing: A review and a model with a nonlocal boundary layer parameterization. *Reviews of Geophysics*, *32*(4), 363–403. https://doi.org/10.1029/94rg01872

Lee, T., Fournier, S., Gordon, A. L., & Sprintall, J. (2019). Maritime Continent water cycle regulates low-latitude chokepoint of global ocean circulation. *Nature Communications*, *10*(1), 1–13. https://doi.org/10.1038/s41467-019-10109-z

Levitus, S., Locarnini, R. A., Boyer, T. P., Mishonov, A. V., Antonov, J. I., Garcia, H. E., & Seidov, D. (2010). *World ocean atlas 2009*.

Li, G., Cheng, L., Zhu, J., Trenberth, K. E., Mann, M. E., & Abraham, J. P. (2020). Increasing ocean stratification over the past half-century. *Nature Climate Change*, *10*(12), 1116–1123. https://doi.org/10.1038/s41558-020-00918-2

Li, M., Gordon, A. L., Gruenburg, L. K., Wei, J., & Yang, S. (2020). Interannual to decadal response of the modelling throughflow vertical profile to Indo-Pacific forcing. *Geophysical Research Letters*, *47*(11), e2020GL087679. https://doi.org/10.1029/2020gl087679

Li, M., Wei, J., Wang, D., Gordon, A. L., Yang, S., Malanotte-Rizzoli, P., & Jiang, G. (2019). Exploring the importance of the Mindoro-Sibutu pathway to the upper-layer circulation of the South China Sea and the Indonesian Throughflow. *Journal of Geophysical Research: Oceans*, *124*(7), 5054–5066. https://doi.org/10.1029/2018jc014910

Liang, L., Xue, H., & Shu, Y. (2019). The Indonesian throughflow and the circulation in the Banda Sea: A modeling study. *Journal of Geophysical Research: Oceans*, *124*(5), 3089–3106. https://doi.org/10.1029/2018jc014926

Liang, W. D., Yang, Y. J., Tang, T. Y., & Chuang, W. S. (2008). Kuroshio in the Luzon Strait. *Journal of Geophysical Research*, *113*(C8). https://doi.org/10.1029/2007jc004609

Liao, G., Yuan, Y., & Xu, X. (2008). Three dimensional diagnostic study of the circulation in the South China Sea during winter 1998. *Journal of Oceanography*, *64*(5), 803–814. https://doi.org/10.1007/s10872-008-0067-4

Linsley, B. K., Rosenthal, Y., & Oppo, D. W. (2010). Holocene evolution of the Indonesian throughflow and the western Pacific warm pool. *Nature Geoscience*, *3*(8), 578–583. https://doi.org/10.1038/ngeo920

Liu, Q., Kaneko, A., & Jilan, S. (2008). Recent progress in studies of the South China Sea circulation. *Journal of Oceanography*, *64*(5), 753–762. https://doi.org/10.1007/s10872-008-0063-8

Liu, Q. Y., Wang, D., Wang, X., Shu, Y., Xie, Q., & Chen, J. (2014). Thermal variations in the South China Sea associated with the eastern and central Pacific El Niño events and their mechanisms. *Journal of Geophysical Research: Oceans*, *119*(12), 8955–8972. https://doi.org/10.1002/2014jc010429

Liu, Z., & Gan, J. (2017). Three-dimensional pathways of water masses in the South China Sea: A modeling study. *Journal of Geophysical Research: Oceans*, *122*(7), 6039–6054. https://doi.org/10.1002/2016jc012511

Liu, Z. J., Minobe, S., Sasaki, Y. N., & Terada, M. (2016). Dynamical downscaling of future sea level change in the western North Pacific using ROMS. *Journal of Oceanography*, *72*(6), 905–922. https://doi.org/10.1007/s10872-016-0390-0

Metzger, E. J., & Hurlburt, H. E. (1996). Coupled dynamics of the South China Sea, the Sulu Sea, and the Pacific Ocean. *Journal of Geophysical Research*, *101*(C5), 12331–12352. https://doi.org/10.1029/95jc03861

Moore, J. K., Fu, W., Primeau, F., Britten, G. L., Lindsay, K., Long, M., et al. (2018). Sustained climate warming drives declining marine biological productivity. *Science*, *359*(6380), 1139–1143. https://doi.org/10.1126/science.aao6379

Nan, F., Xue, H., Chai, F., Wang, D., Yu, F., Shi, M., et al. (2013). Weakening of the Kuroshio intrusion into the South China Sea over the past two decades. *Journal of Climate*, *26*(20), 8097–8110. https://doi.org/10.1175/jcli-d-12-00315.1

Nan, F., Xue, H., & Yu, F. (2015). Kuroshio intrusion into the South China Sea: A review. *Progress in Oceanography*, *137*, 314–333. https://doi.org/10.1016/j.pocean.2014.05.012

Nitani, H. (1972). *Beginning of the Kuroshio. Kuroshio*. Physical Aspect of the Japan Current.

Peliz, Á., Dubert, J., & Haidvogel, D. B. (2003). Subinertial response of a density-driven eastern boundary poleward current to wind forcing. *Journal of Physical Oceanography*, *33*(8), 1633–1650. https://doi.org/10.1175/2415.1

Pörtner, H. O., Roberts, D. C., Masson-Delmotte, V., Zhai, P., Tignor, M., Poloczanska, E., & Petzold, J. (2019). *IPCC special report on the ocean and cryosphere in a changing climate (SROCC)*.

Potemra, J. T., Hautala, S. L., & Sprintall, J. (2003). Vertical structure of Indonesian throughflow in a large-scale model. *Deep Sea Research Part II*, *50*(12–13), 2143–2161. https://doi.org/10.1016/s0967-0645(03)00050-x

Pujiana, K., Gordon, A. L., Sprintall, J., & Susanto, R. D. (2009). Intraseasonal variability in the Makassar Strait thermocline. *Journal of Marine Research*, *67*(6), 757–777. https://doi.org/10.1357/002224009792006115

Qu, T. (2000). Upper-layer circulation in the South China Sea. *Journal of Physical Oceanography*, *30*(6), 1450–1460. https://doi.org/10.1175/1520-0485(2000)030<1450:ulcits>2.0.co;2

Qu, T., Du, Y., & Sasaki, H. (2006b). South China Sea throughflow: A heat and freshwater conveyor. *Geophysical Research Letters*, *33*(23). https://doi.org/10.1029/2006gl028350

Qu, T., Kim, Y. Y., Yaremchuk, M., Tozuka, T., Ishida, A., & Yamagata, T. (2004). Can Luzon Strait transport play a role in conveying the impact of ENSO to the South China Sea? *Journal of Climate*, *17*(18), 3644–3657. https://doi.org/10.1175/1520-0442(2004)017<3644:clstpa>2.0.co;2

Qu, T., & Lukas, R. (2003). The bifurcation of the North Equatorial Current in the Pacific. *Journal of Physical Oceanography*, *33*(1), 5–18. https://doi.org/10.1175/1520-0485(2003)033<0005:tbotne>2.0.co;2

Qu, T. D. (2002). Evidence for water exchange between the South China Sea and the Pacific Ocean through the Luzon Strait. *Acta Oceanologica Sinica*, *21*(2), 175–185.

Qu, T. D., Girton, J. B., & Whitehead, J. A. (2006a). Deepwater overflow through Luzon Strait. *Journal of Geophysical Research*, *111*, C01002. https://doi.org/10.1029/2005JC003139

Qu, T. D., Mitsudera, H., & Yamagata, T. (2000). Intrusion of the North Pacific waters into the South China Sea. *Journal of Geophysical Research*, *105*, 6415–6424. https://doi.org/10.1029/1999JC900323

Qu, Y., Jevrejeva, S., Jackson, L. P., & Moore, J. C. (2019). Coastal Sea level rise around the China Seas. *Global and Planetary Change*, *172*, 454–463. https://doi.org/10.1016/j.gloplacha.2018.11.005

Ramos, R. D., Goodkin, N. F., Druffel, E. R. M., Fan, T. Y., & Siringan, F. P. (2019). Interannual coral $\Delta^{14}C$ records of surface water exchange across the Luzon Strait. *Journal of Geophysical Research: Oceans*, *124*(1), 491–505. https://doi.org/10.1029/2018jc014735

Reynolds, R. W., Rayner, N. A., Smith, T. M., Stokes, D. C., & Wang, W. (2002). An improved in situ and satellite SST analysis for climate. *Journal of Climate*, *15*(13), 1609–1625. https://doi.org/10.1175/1520-0442(2002)015<1609:aiisas>2.0.co;2

Samanta, D., Karnauskas, K. B., & Goodkin, N. F. (2019). Tropical Pacific SST and ITCZ biases in climate models: Double trouble for future rainfall projections? *Geophysical Research Letters*, *46*(4), 2242–2252. https://doi.org/10.1029/2018gl081363

Samanta, D., Karnauskas, K. B., Goodkin, N. F., Coats, S., Smerdon, J. E., & Zhang, L. (2018). Coupled model biases breed spurious low-frequency variability in the tropical Pacific Ocean. *Geophysical Research Letters*, *45*(19), 10–609. https://doi.org/10.1029/2018gl079455

Seager, R., & Simpson, I. R. (2016). Western boundary currents and climate change. *Journal of Geophysical Research: Oceans*, *121*(9), 7212–7214. https://doi.org/10.1002/2016jc012156

Shchepetkin, A. F., & McWilliams, J. C. (2003). A method for computing horizontal pressure-gradient force in an oceanic model with a nonaligned vertical coordinate. *Journal of Geophysical Research*, *108*(C3). https://doi.org/10.1029/2001jc001047

Shchepetkin, A. F., & McWilliams, J. C. (2005). The regional oceanic modelling system (ROMS): A split-explicit, free-surface, topography-following-coordinate oceanic model. *Ocean Modelling*, *9*(4), 347–404. https://doi.org/10.1016/j.ocemod.2004.08.002

Shriver, J. F., & Hurlburt, H. E. (1997). The contribution of the global thermohaline circulation to the Pacific to Indian Ocean throughflow via Indonesia. *Journal of Geophysical Research*, *102*(C3), 5491–5511. https://doi.org/10.1029/96jc03602

Silvy, Y., Guilyardi, É., Sallée, J. B., & Durack, P. J. (2020). Human-induced changes to the global ocean water masses and their time of emergence. *Nature Climate Change*, 1–7. https://doi.org/10.1038/s41558-020-0878-x

Song, Y. T. (2006). Estimation of interbasin transport using ocean bottom pressure: Theory and model for Asian marginal seas. *Journal of Geophysical Research*, *111*(C11). https://doi.org/10.1029/2005jc003189

Sprintall, J., Gordon, A. L., Murtugudde, R., & Susanto, R. D. (2000). A semiannual Indian Ocean forced Kelvin wave observed in the Indonesian seas in May 1997. *Journal of Geophysical Research*, *105*(C7), 17217–17230. https://doi.org/10.1029/2000jc900065

Sprintall, J., Gordon, A. L., Wijffels, S. E., Feng, M., Hu, S., Koch-Larrouy, A., et al. (2019). Detecting change in the Indonesian seas. *Frontiers in Marine Science*, *6*, 257. https://doi.org/10.3389/fmars.2019.00257

Sprintall, J., & Tomczak, M. (1992). Evidence of the barrier layer in the surface layer of the tropics. *Journal of Geophysical Research*, *97*(C5), 7305–7316. https://doi.org/10.1029/92jc00407

Sprintall, J., Wijffels, S. E., Molcard, R., & Jaya, I. (2009). Direct estimates of the Indonesian Throughflow entering the Indian Ocean: 2004–2006. *Journal of Geophysical Research*, *114*(C7). https://doi.org/10.1029/2008jc005257

Suga, T., Kato, A., & Hanawa, K. (2000). North Pacific Tropical Water: Its climatology and temporal changes associated with the climate regime shift in the 1970s. *Progress in Oceanography*, *47*(2–4), 223–256. https://doi.org/10.1016/S0079-6611(00)00037-9

Susanto, R. D., Ffield, A., Gordon, A. L., & Adi, T. R. (2012). Variability of Indonesian throughflow within Makassar Strait, 2004–2009. *Journal of Geophysical Research*, *117*(C9). https://doi.org/10.1029/2012jc008096

Susanto, R. D., & Gordon, A. L. (2005). Velocity and transport of the Makassar Strait throughflow. *Journal of Geophysical Research*, *110*(C1). https://doi.org/10.1029/2004jc002425

Susanto, R. D., Gordon, A. L., Sprintall, J., & Herunadi, B. (2000). Intraseasonal variability and tides in Makassar Strait. *Geophysical Research Letters*, *27*(10), 1499–1502. https://doi.org/10.1029/2000gl011414

Susanto, R. D., Wei, Z., Adi, R. T., Fan, B., Li, S., & Fang, G. (2013). Observations of the Karimata Strait throughflow from December 2007 to November 2008. *Acta Oceanologica Sinica*, *32*(5), 1–6. https://doi.org/10.1007/s13131-013-0307-3

Susanto, R. D., Wei, Z., Adi, T. R., Zheng, Q., Fang, G., Fan, B., & Setiawan, A. (2016). Oceanography surrounding Krakatau Volcano in the Sunda Strait, Indonesia. *Oceanography*, *29*(2), 264–272. https://doi.org/10.5670/oceanog.2016.31

Tian, J., Yang, Q., Liang, X., Xie, L., Hu, D., Wang, F., & Qu, T. (2006). Observation of Luzon Strait transport. *Geophysical Research Letters*, *33*(19). https://doi.org/10.1029/2006gl026272

Toste, R., de Freitas Assad, L. P., & Landau, L. (2019). Changes in the North Pacific Current divergence and California Current transport based on HadGEM2-ES CMIP5 projections to the end of the century. *Deep Sea Research Part II: Topical Studies in Oceanography*, *169*, 104641. https://doi.org/10.1016/j.dsr2.2019.104641

Tozuka, T., Qu, T., Masumoto, Y., & Yamagata, T. (2009). Impacts of the South China Sea throughflow on seasonal and interannual variations of the Indonesian throughflow. *Dynamics of Atmospheres and Oceans*, *47*(1–3), 73–85. https://doi.org/10.1016/j.dynatmoce.2008.09.001

Tozuka, T., Qu, T., & Yamagata, T. (2007). Dramatic impact of the South China Sea on the Indonesian throughflow. *Geophysical Research Letters*, *34*(12). https://doi.org/10.1029/2007gl030420

Voldoire, A., Saint-Martin, D., Sénési, S., Decharme, B., Alias, A., Chevallier, M., et al. (2019). Evaluation of CMIP6 deck experiments with CNRM-CM6-1. *Journal of Advances in Modeling Earth Systems*, *11*(7), 2177–2213. https://doi.org/10.1029/2019ms001683

Wajsowicz, R. C. (1999). Models of the Southeast Asian seas. *Journal of Physical Oceanography*, *29*(5), 986–1018. https://doi.org/10.1175/1520-0485(1999)029<0986:motsas>2.0.co;2

Wang, Q., Cui, H., Zhang, S., & Hu, D. (2009). Water transports through the four main Straits around the South China Sea. *Chinese Journal of Oceanology and Limnology*, *27*(2), 229–236. https://doi.org/10.1007/s00343-009-9142-y

Wang, X. W., Liu, Z. Y., & Peng, S. Q. (2017). Impact of tidal mixing on water mass transformation and circulation in the South China Sea. *Journal of Physical Oceanography*, *47*(2), 419–432. https://doi.org/10.1175/Jpo-D-16-0171.1

Wang, Y., Fang, G., Wei, Z., Qiao, F., & Chen, H. (2006). Interannual variation of the South China Sea circulation and its relation to El Niño, as seen from a variable grid global ocean model. *Journal of Geophysical Research*, *111*(C11). https://doi.org/10.1029/2005jc003269

Wang, Y., Xu, T., Li, S., Susanto, R. D., Agustiadi, T., Trenggono, M., & Wei, Z. (2019). Seasonal variation of water transport through the Karimata Strait. *Acta Oceanologica Sinica*, *38*(4), 47–57. https://doi.org/10.1007/s13131-018-1224-2

Wei, Z., Li, S., Susanto, R. D., Wang, Y., Fan, B., Xu, T., et al. (2019). An overview of 10-year observation of the South China Sea branch of the Pacific to Indian Ocean throughflow at the Karimata Strait. *Acta Oceanologica Sinica*, *38*(4), 1–11. https://doi.org/10.1007/s13131-019-1410-x

Wei, Z. H. A. O., Hou, Y. J., Peng, Q. I., Le, K. T., & Li, M. K. (2009). The effects of monsoons and connectivity of South China Sea on the seasonal variations of water exchange in the Luzon Strait. *Journal of Hydrodynamics, Ser. B*, *21*(2), 264–270.

Wijffels, S. E., Meyers, G., & Godfrey, J. S. (2008). A 20-yr average of the Indonesian Throughflow: Regional currents and the interbasin exchange. *Journal of Physical Oceanography*, *38*(9), 1965–1978. https://doi.org/10.1175/2008jpo3987.1

Williams, K. D., Copsey, D., Blockley, E. W., Bodas-Salcedo, A., Calvert, D., Comer, R., et al. (2018). The Met Office global coupled model 3.0 and 3.1 (GC3. 0 and GC3. 1) configurations. *Journal of Advances in Modeling Earth Systems*, *10*(2), 357–380. https://doi.org/10.1002/2017ms001115

Wu, C. R. (2013). Interannual modulation of the Pacific Decadal Oscillation (PDO) on the low-latitude western North Pacific. *Progress in Oceanography*, *110*, 49–58. https://doi.org/10.1016/j.pocean.2012.12.001

Wu, J., Lao, Q., Chen, F., Huang, C., Zhang, S., Wang, C., & Lu, X. (2021). Water mass processes between the South China Sea and the Western Pacific through the Luzon Strait: Insights from hydrogen and oxygen isotopes. *Journal of Geophysical Research: Oceans*, e2021JC017484.

Wyrtki, K. (1961). *Physical Oceanography of the Southeast Asian Waters* (Vol. 2). University of California, Scripps Institution of Oceanography.

Xie, S. P., Xie, Q., Wang, D., & Liu, W. T. (2003). Summer upwelling in the South China Sea and its role in regional climate variations. *Journal of Geophysical Research*, *108*(C8). https://doi.org/10.1029/2003jc001867

Xu, H. Z., Xu, J. D., Li, L., Chen, J., Du, Y., & Wang, D. X. (2007). Hydrography and circulation characteristics about the northeast area of South China Sea during March 2001. *Acta Oceanologica Sinica*, *29*(15), 10–20.

Xu, J. P. (2004). Several characteristics of water exchange in the Luzon Strait. *Acta Oceanologica Sinica*, *23*(1), 11–21.

Xu, T. F., Wei, Z. X., Susanto, R. D., Li, S. J., Wang, Y. G., Wang, Y., & Fang, G. H. (2021). Observed water exchange between the South China Sea and Java Sea through Karimata Strait. *Journal of Geophysical Research: Oceans*, e2020JC016608. https://doi.org/10.1029/2020jc016608

Xue, H. J., Chai, F., Pettigrew, N., Xu, D. Y., Shi, M., & Xu, J. P. (2004). Kuroshio intrusion and the circulation in the South China Sea. *Journal of Geophysical Research*, *109*, C02017. https://doi.org/10.1029/2002JC001724

You, Y. Z., Chern, C. S., Yang, Y., Liu, C. T., Liu, K. K., & Pai, S. C. (2005). The South China Sea, a cul-de-sac of North Pacific Intermediate Water. *Journal of Oceanography*, *61*(3), 509–527. https://doi.org/10.1007/s10872-005-0059-6

Yu, L., Jin, X., & Weller, R. A. (2008). Multidecade global flux datasets from the objectively analyzed air-sea fluxes (oaflux) project: Latent and sensible heat fluxes, ocean evaporation, and related surface meteorological variables lisan yu. *OAFlux Project Technical Report*, 74.

Yuan, Y., Liao, G., Kaneko, A., Yang, C., Zhu, X. H., Chen, H., et al. (2012). Currents in the Luzon Strait obtained from moored ADCP observations and a diagnostic calculation of circulation in spring 2008. *Dynamics of Atmospheres and Oceans*, *58*, 20–43. https://doi.org/10.1016/j.dynatmoce.2012.07.002

Yuan, Y., Liao, G., Yang, C., Liu, Z., Chen, H., & Wang, Z. G. (2014). Summer Kuroshio Intrusion through the Luzon Strait confirmed from observations and a diagnostic model in summer 2009. *Progress in Oceanography*, *121*, 44–59. https://doi.org/10.1016/j.pocean.2013.10.003

Zeng, L., & Wang, D. (2017). Seasonal variations in the barrier layer in the South China Sea: Characteristics, mechanisms and impact of warming. *Climate Dynamics*, *48*(5–6), 1911–1930. https://doi.org/10.1007/s00382-016-3182-8

Zeng, L., Wang, D., Chen, J., Wang, W., & Chen, R. (2016). SCSPOD14, A South China Sea physical oceanographic dataset derived from in situ measurements during 1919–2014. *Scientific data*, *3*, 160029. https://doi.org/10.1038/sdata.2016.29

Zhai, F., & Hu, D. (2013). Revisit the interannual variability of the North Equatorial Current transport with ECMWF ORA-S3. *Journal of Geophysical Research: Oceans*, *118*(3), 1349–1366. https://doi.org/10.1002/jgrc.20093

Zhang, H. (2018). Fisheries cooperation in the South China Sea: Evaluating the options. *Marine Policy*, *89*, 67–76. https://doi.org/10.1016/j.marpol.2017.12.014

Zhang, Z., Tian, J., Qiu, B., Zhao, W., Chang, P., Wu, D., & Wan, X. (2016). Observed 3D structure, generation, and dissipation of oceanic mesoscale eddies in the South China Sea. *Scientific Reports*, *6*, 24349. https://doi.org/10.1038/srep24349

Zhao, W., Zhou, C., Tian, J. W., Yang, Q. X., Wang, B., Xie, L. L., & Qu, T. D. (2014). Deep water circulation in the Luzon Strait. *Journal of Geophysical Research: Oceans*, *119*, 790–804. https://doi.org/10.1002/2013JC009587

Zhou, H., Nan, F., Shi, M., Zhou, L., & Guo, P. (2009). Characteristics of water exchange in the Luzon Strait during September 2006. *Chinese Journal of Oceanology and Limnology*, *27*(3), 650–657. https://doi.org/10.1007/s00343-009-9175-2

Zhou, H., Yuan, D., Li, R., & He, L. (2010). The western South China Sea currents from measurements by Argo profiling floats during October to December 2007. *Chinese Journal of Oceanology and Limnology*, *28*(2), 398–406. https://doi.org/10.1007/s00343-010-9052-z

Zhu, Y., Sun, J., Wang, Y., Li, S., Xu, T., Wei, Z., & Qu, T. (2019). Overview of the multi-layer circulation in the South China Sea. *Progress in Oceanography*, *175*, 171–182. https://doi.org/10.1016/j.pocean.2019.04.001